University of Pretoria

Towards controlled release of a natural mosquito repellent from polymer matrices

Mohamed Ubaid Akhtar

A dissertation submitted in partial fulfilment of the requirements for the
degree of
MASTER OF SCIENCE (APPLIED SCIENCE: CHEMICAL TECHNOLOGY)
In the
FACULTY OF ENGINEERING
UNIVERSITY OF PRETORIA

December 2014

DISSERTATION

Towards controlled release of a natural mosquito repellent from polymer matrices

M U Akhtar

Supervisor: Professor Walter W. Focke

Department: Chemical Engineering

University: University of Pretoria

Degree: Master of Science (Applied Science: Chemical Technology)

Synopsis

Malaria is still the most important parasitic disease in humans with most cases occurring in Sub-Saharan Africa (90% cases). It is transmitted via anopheles mosquitoes. Several vector control methods are available, e.g. long lasting insecticidal mosquito nets (LLINs), insecticide-treated nets (ITNs) and indoor residual spraying (IRS). However, they are effective only when a person is indoors. Outdoor protection can be obtained for short periods (48-72 hours) using topical repellents. This preliminary study investigated the possibility to develop longer acting delivery forms based on polymer technology. The viability of two different approaches were considered for the controlled release of the natural repellent 3,7-dimethyloct-6-en-1-al (citronellal). The first idea was to dissolve the repellent in the polymer while controlling the rate of release by clay nanoplatelets dispersed in the matrix. Towards this, ethylene vinyl acetate (EVA) copolymer (18% VA) was modified with organically modified nanoclay. Release tests showed that this approach was not viable as only a small amount

of repellent could be incorporated and it was lost within a day or two from thin polymer strands.

The second approach targeted the use of a polymer in which the repellent is not soluble at ordinary temperature but where solubility is achieved at high temperatures. In this case polyethylene was used as host polymer. It was shown that large quantities of repellent can be trapped inside the polymer matrix using the temperature induced phase separation method (TIPS). Scanning electron microscopy revealed that a microporous co-continuous phase structure was obtained by shock cooling homogeneous mixtures to temperatures well below the spinodal phase boundary curve.

The phase behaviour of the LLDPE-citronellal system was studied using cloud point determinations in a microscope fitted with a hot stage and by differential scanning calorimetry. The experimental data points on the bimodal phase envelope were used to fix parameter values of the Flory-Huggins equation. The latter was then used to predict the location of the spinodal lines. At 40 wt.% polymer the spinodal boundary is located at 96 °C. However, experiments showed that quenching temperature of 5°C (i.e. the temperature of typical cooling baths used during filament extrusion) is sufficient to generate the desired microporous structure.

Key words: EVA; Citronellal; Organoclay; nanocomposite; malaria;

ACKNOWLEDGEMENT

I wish to express my appreciation to the following organisations and persons who made this dissertation possible:

a) This dissertation is based on a research project of Malaria Vector Control. Permission to use the material is gratefully acknowledged. I would like to extend my appreciation to the following person for making this project a success and for all his guidance, support and encouragement:

    i) Prof Walter W. Focke (Project supervisor)

b) The University of Pretoria and National Research Foundation (NRF) for financial support, the provision of data and the use of laboratory facilities during the course of the study.

c) The following persons are gratefully acknowledged for their assistance during the course of the study:

    i)   Isbe van der Westhuizen (Thermal analysis, DSC and optical microscopy)

    ii)   Gerard Jacob Puts (Thermal analysis)

    iii)   Wiebke Grote (X-Ray Diffraction analysis)

d) My family and friends for their guidance, encouragement and support during the study.

Table of Contents

List of Tables

List of Figures

List of Nomenclature

Symbols	Property [Unit]
d_{001}	Interlayer thickness of clay [nm]
h	thickness of a single (exfoliated) clay platelet [nm]
ϕ	volume fraction [-]
P_p	permeability coefficient of the polymer [m^2]
j	Flux [mol·m^{-2}·s^{-1}]
d	Thickness of a film [m]
Δp	Pressure difference [N/m^2]
P_c	permeability coefficient of gas/liquid molecules [m^2]
L	length of silicate platelets [nm]
W	Width of silicate platelets [nm]
ξ	dispersion spacing between two platelets [nm]
θ	orientation of silicate platelets [°]
τ	tortuous factor [-]
P_r	relative permeability [-]
S	order parameter [-]
ΔH_{mix}	change in enthalpy of mixing [J]
ΔS_{mix}	change in entropy of a mixing [J/K]
ΔG_{mix}	change in Gibb's free energy of mixing [J/mol]
R	Universal gas constant [J/(mol.K)]
T	Absolute temperature [K]
n_1	numbers of moles of solvent [mol]
n_2	numbers of moles of polymer [mol]
X_1	mole fraction of solvent [-]
X_2	mole fraction of polymer [-]
N_1	Number of solvent molecules [-]

N_2	Number of polymer molecules [-]
ϕ_1	Volume fraction of solvent [-]
ϕ_2	Volume fraction of polymer [-]
χ	Flory – Huggins Interaction parameter [-]
x	Total number of segments in a polymer chain [-]
N_A	Avogadro's number [-]
a	Entropic component of χ [J]
b	Enthalpic component of χ [J/K]
μ_1	Chemical potential of solvent [J/mol]
μ_2	Chemical potential of polymer [J/mol]
T_c	Critical absolute temperature [K]
ϕ_{2c}	Critical concentration of polymer [-]
α	Solvent rich phase [-]
β	Polymer rich phase [-]
M_1	Molar mass of solvent [kg/mol]
$M_{n.2}$	Number average molecular mass of polymer [kg/mol]
$M_{w.2}$	Weight average molecular mass [kg/mol]
ρ_1	Density of solvent [kg/m^3]
ρ_2	Density of polymer [kg/m^3]
χ_{crit}	Critical Flory-Huggins interaction parameter [-]
ΔH_u	Heat of fusion or crystallization [J/mol]
$D_{M.2}$	Molar mass dispersity [-]
V_1	Volume of solvent [m^3]
V_2	Volume of polymer [m^3]
V_0	Volume of a lattice site [m^3]

List of Acronyms

LLINs	Long lasting insecticidal mosquito nets
ITNs	Insecticide-treated nets
IRS	Indoor residual spraying
EVA	Ethylene Vinyl Acetate Copolymer
LLDPE	Linear low density polyethylene
TGA	Thermal Gravimetric Analysis
XRD	X-Ray Diffraction
FESEM	Field Emission Scanning Electron Microscopy
WHO	World Health Organization
RBM	Roll Back Malaria
DEET	N,N-Diethyl-m-toluamide
Citronellal	3,7-dimethyloct-6-en-1-al
Citriodiol	p-menthane-3,8-diol
MMT	Montmorillonite
CEC	Critical exchange capacity
FF	face-to-face
FE	face-to-edge
EE	edge-to-edge
PP	Polypropylene
SIPS	Solvent induced phase separation
NIPS	Non-Solvent induced phase separation
TIPS	Thermally induced phase separation
TAEPS	Thermally assisted evaporation phase separation
PE	Polyethylene
LDPE	Low-density polyethylene
HDPE	High-density polyethylene
L-L	Liquid–liquid

F-H	Flory-Huggins
UCST	Upper critical solution temperature
LCST	Lower critical solution temperature
DMBHTA	Dimethyl benzyl hydrogenated tallow ammonium
DSC	Differential scanning calorimetry
OM	Hot stage optical microscopy
UNICEF	United Nations International Children's Emergency Fund
UNDP	United Nations Development Program

1. Introduction

1.1 Background

In recent years, a great deal of research has been carried out in order to control the spread of Malaria. It is one of the most serious vector-borne diseases that have taken millions of lives over the years mainly in the tropical areas. According to the World Health Organization (WHO) malaria report (2013), over 627,000 people died in 2012. The main victims were children under five years of age in Africa. However, Murray et al. (Murray et al., 2012) believe that the malaria mortality burden is larger than previously estimated, especially in adults. Their study assessed that in 2010 malaria was the cause of 1.24 million deaths compared to 655,000 deaths reported by the WHO. In the tropical region of African infant mortality (children< 5 years old) was found to be 24% versus 16% of the WHO malaria report findings (2011). Figure 1 illustrates the significance of these observations.
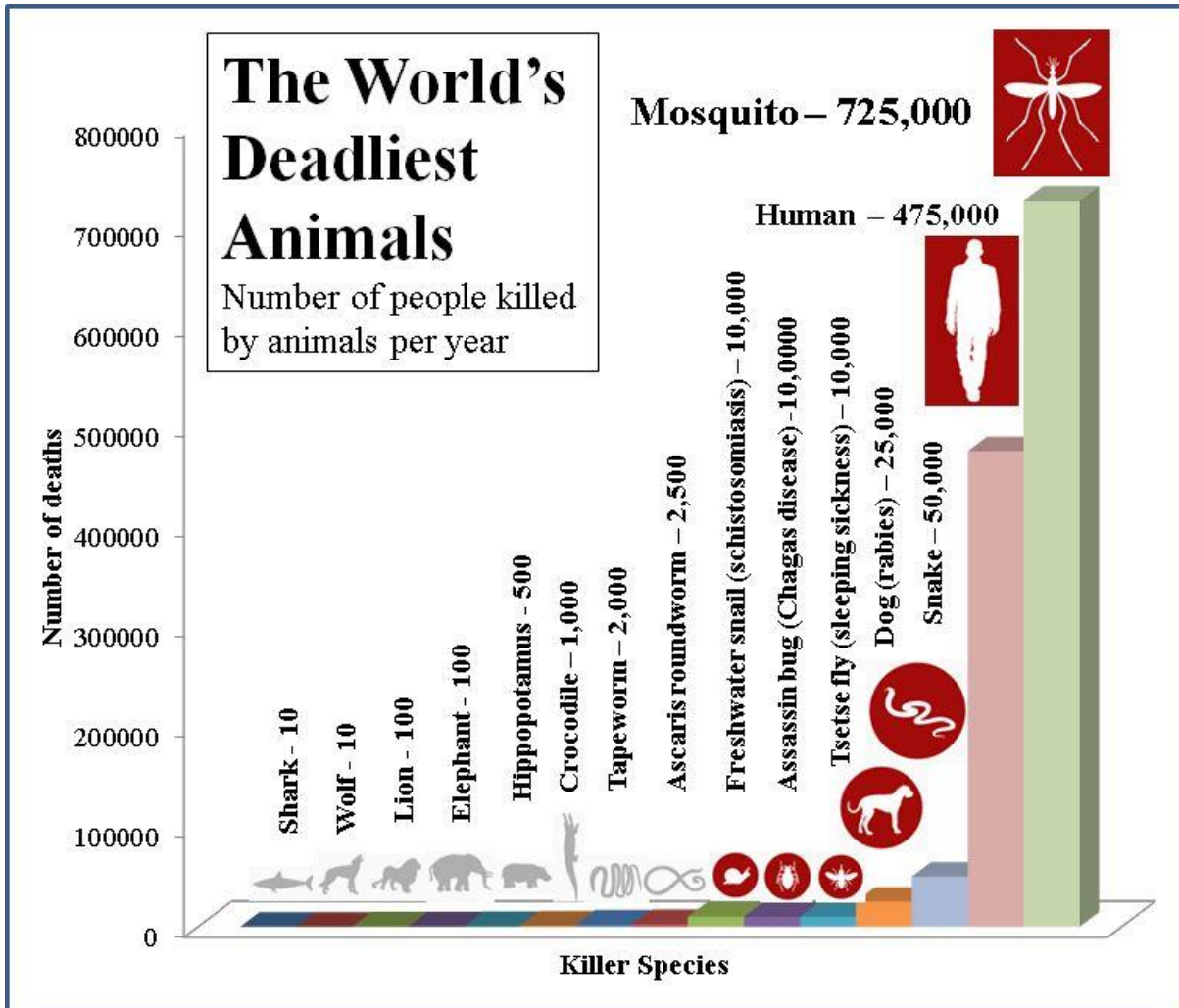
SOURCES: WHO; crocodile-attack.info; Kasturiratne et al. (doi.org/10.1371/journal.prned.0050218); FAO (webcitation.org/6OgpS8SVO); Linnell et al. (webcitation.org/6ORL7DBUO); Packer et al. (doi.org/10.1038%2F436927a); Alessandro De Maddalena. All calculations have wide error margins

Figure 1: Number of people killed by animals per year

There are many institutes, governmental and non-governmental, that aim to eliminate or at least reduce malaria to a minimal level. In this regard, the Roll Back Malaria (RBM) Initiative was launched in 1998 by WHO and several UN agencies such as the World Bank, UNICEF and UNDP. Their stated goal was to halve the deaths of people due to malaria by 2010. Therefore, strategic plans were introduced to increase the capacity for Malaria interventions worldwide and different routes like social marketing, NGOs groups, and village shops were used to efficiently supply drugs, insecticide treated materials etc. to communities (Roll Back Malaria, 2000).

In a global public health context, the genus Anopheles is the most important group of pathogen-carrying mosquitoes due to their exclusive participation in the transmission of human malaria parasites. This parasite is also called Plasmodium Falciparum.

According to the research (Trape et al., 2011), Anopheles female mosquitoes require a blood meal as a source of proteins in order for their eggs to mature. These species normally attack after sunset and biting reaches its peak at midnight. In their study, they initially used anti-malarial therapies in order to reduce morbidity numbers and then after few years followed up with the introduction of bed nets in the areas under study. Amazingly, the strategy worked for seven to eight months where the morbidity and mortality cases were brought down by 40 to 50 %. However, after that period, the morbidity cases started to rise up again which showed that the mosquitoes changed their biting routine and they were biting before a person could go under the bed net.

Similar behaviour was recently found in Kenya where an unknown species of mosquito whose DNA does not match with any of the existing species of mosquitoes (Jennifer and Stevenson, 2012).

This is an alarming situation. On the one hand, researchers are dealing with the existing species of mosquitoes which are not changing their biting routine but are developing increased resistance to currently used insecticides and anti-malarial therapies. On the other hand, unknown mosquito's species and mutations are emerging whose characteristics are as yet unknown (Jennifer and Stevenson, 2012, Namountougou et al., 2013, Lizin et al., 2013). In this situation, using an Integrated Management System (Nancy Fullman, 2013, http://www.ivmproject.net/) can be a useful tool where the studies are focused on the interventions of different malaria vector control methods.

Mosquito borne disease types include West Nile fewer, filariasis, dengue fever, yellow fewer and others. One of the best ways to reduce the transmission and thus incidence of these infectious diseases is to suppress mosquito numbers. This is supported by the decrease over the last few years of the incidence of malaria owing to the implementation of residual indoor spray (IRS) and long-life insecticide bed nets (LLINs) in Africa (WHO) (2013). Both these interventions target mosquitoes that feed indoors. However, mosquitoes become active in the afternoon. This means that a considerable amount of biting is happening while still outside especially on the ankles. Thus people must also be protected when still outdoors.

This is possible through the use of topical mosquito repellents, i.e. substances that are applied to the skin that discourage insects from approaching. Typically these provide protection for at most a few hours. N,N-Diethyl-m-toluamide (DEET) is the most widely used insect repellent in current use. However, its use has become controversial and the search is on for an environmentally friendly alternative. Several new compounds, including some derived from renewable resources, are currently under review. Citriodiol (p-menthane-3,8-diol) is a good example. It is recognized as the only effective naturally derived substance for deterring mosquitoes carrying West Nile Virus. However, this and other alternative repellents are much more volatile than DEET. Due to this their effectiveness only lasts for few hours. Since most people in Africa live in poverty, they cannot afford to use such products on a daily basis.

Products that are used for outdoors control include mosquito/larvae traps, repelling candles, repelling ointments, ankle bracelets etc. All these products are focusing on using naturally occurring repellents which only last for few hours (48 – 72 hours), as shown in Figure 2.

Figure 2: Some of the products used for repellency of mosquitoes at outdoor

Therefore, there is a need of products that can deliver slow release of naturally occurring mosquito repellents over extended periods of time without affecting their repellence performance. This means that ways must be found to reduce the release rate of such compounds. In this regard it is important to keep in mind that the repellents are usually liquids at body temperature.

It would be advantageous to use systems that will provide protection for much longer time periods. However, there is a limit to the amount of repellents that can be applied via skin creams and lotions. Clothing impregnated with permethrin provides longer term protection and it is use by the US military. Permethrin is an insecticide but it also has repellent activity. However, skin contact needs to be avoided.

An interesting concept is offered by insecticidal ankle bracelets or the straps on low cost shoes, e.g. slip-slops that can be distributed to rural communities in a way similar to the system currently operated for bed nets. These polymer products can act as reservoirs for suitable repellents. One possibility is to trap larger quantities of the active ingredients inside the polymer matrix. Over time the repellent may be released via the blooming mechanism illustrated in Figure 3.
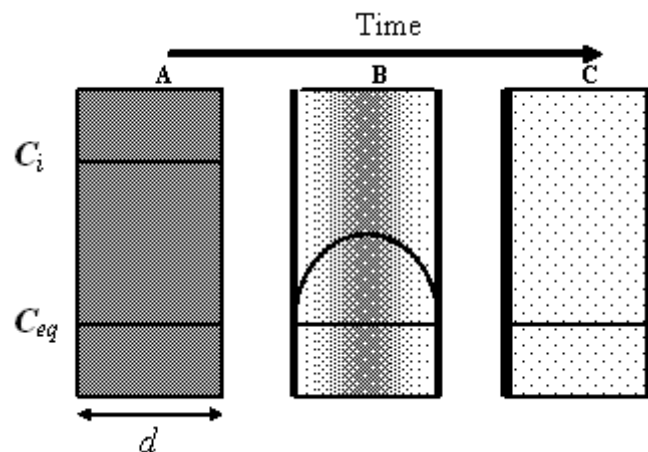
Figure 3: Schematic of the surface blooming mechanism in from a polymer filament with diameter d.

The intensity of the grey colour scales with the repellent concentration. Immediately after formation of the filament, the active is homogeneously dispersed throughout the amorphous regions in the filament (State A). The concentration C_i is determined by the dosage and exceeds the equilibrium concentration C_{eq}. The additive diffuses to the surface setting up a concentration profile inside the fibre (State B). Ultimately, after a sufficiently long time, the concentration inside the fibre is reduced to a homogeneous concentration equal to the solubility limit C_{eq} (State C) while the excess repellent has accumulated on the outside surface.

A disadvantage of this approach is the fact that there will be an exponential decay of the release rate over time. Initially the release rate will be higher than needed and later it will be insufficient. Another disadvantage is that there will be a limit to the solubility of the liquid active in the polymer matrix. Furthermore, if the active is dissolved in the matrix, it implies that the polymer will be in a swollen state initially. This means that the polymer will progressively shrink as the active is released and this has implications for the dimensional stability of the product.

1.1. Aim

The ultimate aim of this research is to design and develop polymer products based on naturally occurring insecticides or repellents that can be used outdoor in a safer and convenient way for longer periods and yet low cost. This particular project was a preliminary study aimed at testing concepts that could lead to such a product.

1.2. Objective

The objectives of this project were:

- Review the literature and generate scientific data to develop the understanding needed to let polymer materials retain large amounts of repellents and release them at an effective rate for long periods of time.
- Consider organoclays based on readily available clays to inhibit the release of a volatile active from a polymer matrix. This could facilitate controlled release of the active ingredients, and
- Determine whether microporous polymers can trap large amounts of a volatile repellent, specifically citronellal.
- Future work needs to focus on the design and manufacture prototype products with particular emphasis on using natural products as active ingredients and polymers based on renewable resources.

2. Literature Review

This literature review is a combination of the work done in the first study and the work done following the results of the first study given in Section 2.1 and Section 2.3 respectively.

For the first idea, it is imperative to understand the physical properties of nano-clay particles and their role in polymers and the problems in relation to the dispersion at nano-scale achieving intercalation/exfoliation.

In the second idea, it is important to understand the phase separation behaviour of polymer solutions and be able to apply the Flory-Huggins lattice model on thermally induced phase separation technique.

2.1. Clay Nanocomposites
2.1.1. Clay Minerals (Definitions)

Clays are categorized into two broad classes according to their interlayer charges: anionic clays and cationic clays. The anionic clays or mixed metal hydroxides are difficult to find but are simple and inexpensive to synthesis compared to the cationic clays which are widespread in nature (Reichle, 1986, Vaccari, 1998).

Cationic clays are layered silicates built of two structural units. The 1:1 structures (e.g. in kaolinite) are the simplest, where a silica tetrahedral sheet is bonded to an aluminium octahedron, sharing the oxygen atoms. However, for the preparation of polymer nanocomposites, the layered silicates are commonly employed belong to the family of 2:1 phyllosilicates or smectites. Their crystal structure consists of stacked layers made of two silica tetrahedrons fused to an edge-shared octahedral sheet of alumina (Figure 4).
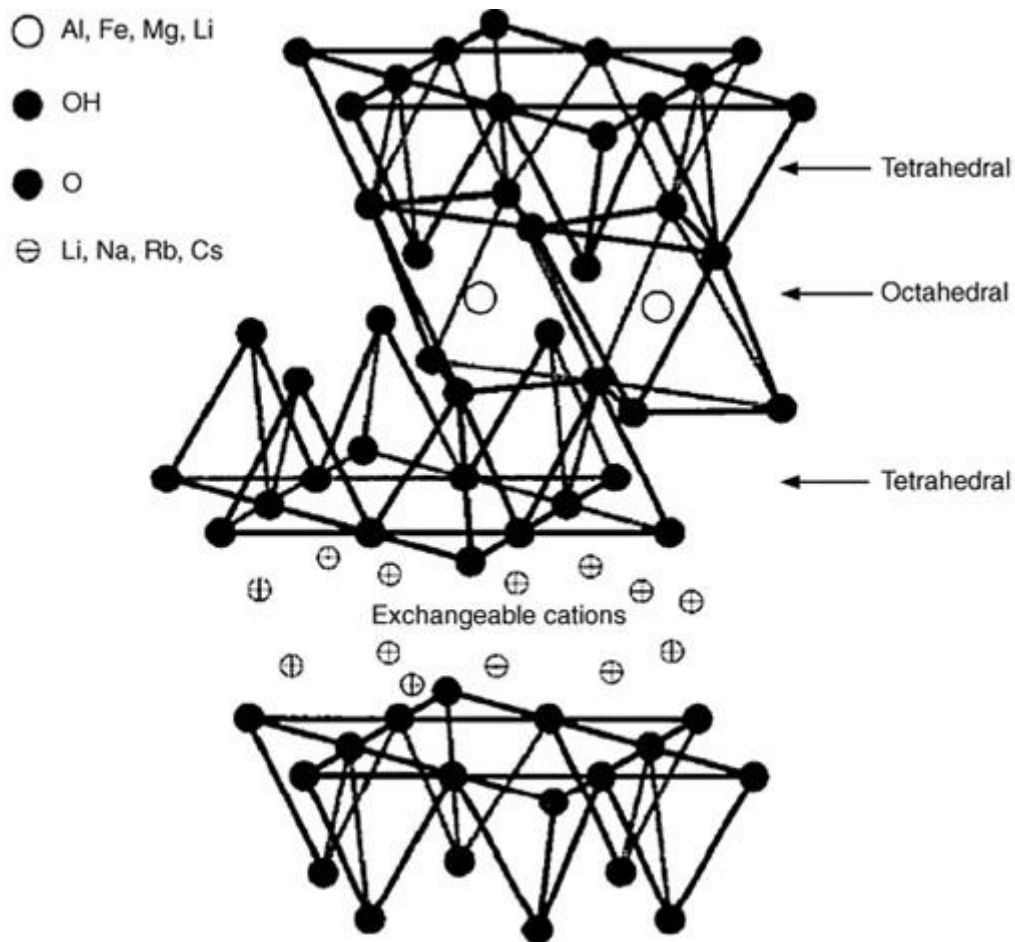
Figure 4: The structure of 2:1 layered silicates (Sinha Ray and Okamoto, 2003)

The layer thickness is nearly 1nm and the lateral dimensions may differ from 300Å to several microns, giving an aspect ratio (length/thickness) greater than 1000. The neighbouring layers are separated by a regular van der Waals gap, called the interlayer or gallery. Isomorphic substitution within the layers generates negative charges that are normally counterbalanced by sodium or calcium ions, existing hydrated in the interlayer (Newman, 1986, Vaccari, 1998, Bergaya et al., 2006).

According to (Bergaya et al., 2006), the clay minerals properties are usually related with those of smectites and are characterized by, (i) a layered structure with one dimension in the nanometer range, (ii) anisotropy of the layers, (iii) different types of surface (basal, edge and interlayer), (iv) cation and anion

exchange capacity relatively easy chemical, physical or thermal modification, (v) interlayer swelling in appropriate solvents, and (vi) plasticity.

Two particular characteristics of layered silicates play an important role in the creation of nanocomposites: the first is the ability of silicate sheets to disperse into individual layers, and the second is the possibility to modify their surface chemistry through ion exchange reactions with organic and inorganic cations.

2.1.2. Types of Clay Minerals

Clay Minerals can be divided into different families which are as follows (Utracki, 2004):

- Kaolins
- Serpentines
- Illite Group (Micas)
- Chlorites and Vermiculites
- Glauconite
- Sepiolite, Palygorskite and Attapulgite
- Smectites or Phyllosilicates
  - Bentonite
  - Montmorillonite (MMT)

2.1.2.1. *Montmorillonite*

Montmorillonite (MMT) is the name specified for clay found near Montmorillonite in France, where it was identified by Knight in 1896. It is the most common smectite used for the production of commercial Polymer Nanocomposites. The idealized structure of Na-MMT is shown in Figure 5.
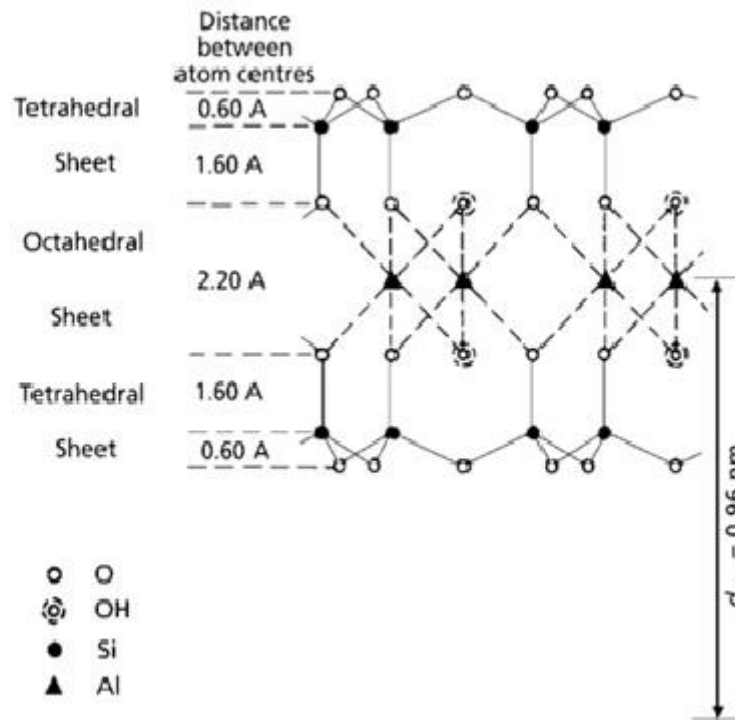
Figure 5: Idealized structure of dry phyllosilicate with the unit cell: $[Al_2(OH)_2(Si_2O_5)_2]_2$ + 5 wt.% H_2O. The unit cell molecular weight is 720 + water and counter ions (e.g., Na^+); the minimum d_{001} spacing for dry MMT is 0.96 nm (the inter-lamellar gallery height 0.30 nm), the surface area of the unit cell is $0.458nm^2$ (Olphen and Fripiat, 1979).

The unit cell is usually written as:

Triple layer sandwich of two silica tetrahedron sheets and a central octahedral sheet with 0.67 negative charges per unit cell	$[Al_{3.33}Mg_{0.67}]^{-(0.67)}Si_8O_{20}(OH)_4$ $\downarrow$
Aqueous inter-lamellar layer containing 0.67 Na^+ cations per unit cell	$(n \times H_2O)Na_{0.67}^+$
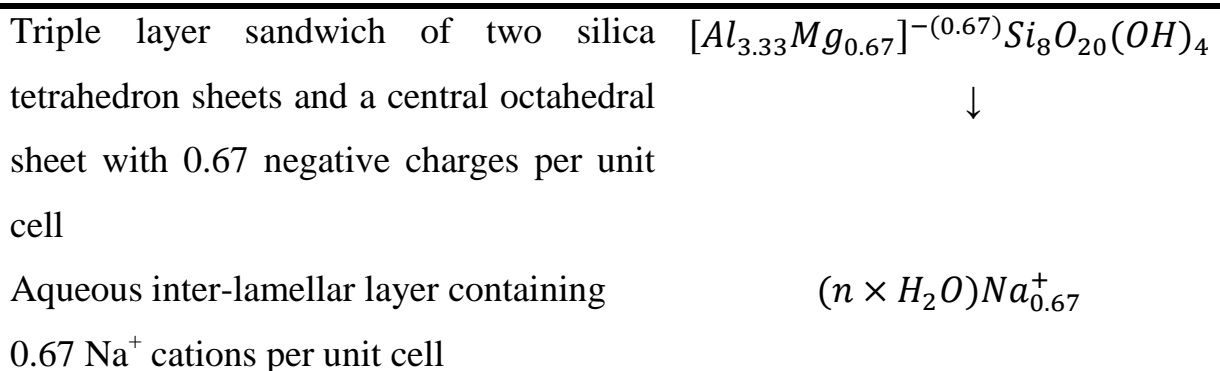
Thus, an idealized MMT has 0.67 units of negative charge per unit cell and it behaves as a weak silicic acid. Since the molecular weight of a unit cell is $M = 734$ + water, the critical exchange capacity (CEC) of idealized MMT is: CEC =

0.915 meq/g (one ion per 1.36 nm^2), i.e., the anionic groups are spaced about 1.2 nm apart. The charge is located on the flat surface of the platelets and a small positive charge is also present at the edges.

The specific surface area of MMT is A_{sp} = 750-800 m^2/g (theoretical value is 834 m^2/g). From the cited values it follows that the density of the triple sandwich is 4.03 g/ml and that the inter-lamellar gallery thickness is 0.79 nm, hence the interlayer thickness of hydrated MMT should be d_{001} = 1.45 nm and the average density = 2.385 g/ml. Drying MMT at 150 °C reduces the gallery height to 0.28 nm (which corresponds to a water monolayer), hence the interlayer spacing decreases to d_{001} = 0.94 nm and the average density increases to 3.138 g/ml. Assuming that MMT platelets are fully exfoliated and that locally they are parallel to each other, the interlayer spacing h should be inversely proportional to the clay volume fraction, ϕ,

$$d_{001} = h/\phi \tag{1}$$

where $h \cong 0.96$ nm is the thickness of a single (exfoliated) clay platelet. This simple relation predicts the interlayer thickness of clay (Utracki, 2004).

2.1.2.1.1.   Properties and Applications of Montmorillonite

Commercially, MMT is supplied in the form of powder with about an 8 μm particle size, each containing about 3000 platelets with a moderate aspect ratio p = 10 to 300. Typical properties and applications are listed in **Table 1**.

Table 1: Properties and Applications of Montmorillonite (Grimshaw, 1980)

Physical Constants		Applications
Unit cell molecular wt. (g/mol)	540.46	To slow down water flow through soil
Density (g/ml)	2.3 to 3.0	To produce nanocomposites
Crystal system	Monoclinic	To de-colour and purify liquids, viz. wines, juices etc.
Moh's hardness @ 20°C	1.5 - 2.0	As filler for paper or rubber
Appearance	White, yellow or brown with dull luster	In drilling muds to give the water greater viscosity
Cleavage	Perfect in one direction, lamellar	As a base for cosmetics and drugs
		As an absorbent
Characteristic	In H_2O its volume expands up to 30-folds	As a base for pesticides and herbicides
Field indicators	Softness and soapy feel	As food additive for poultry and pet foods
		For thickening of lubricating oils and greases
DSC endothermic peak, T (°C)	140, 700, 875	For binding foundry sands
DSC exothermic peak, T (°C)	920	To generate thixotropy
MMT swells in water more than any other mineral	Largest for Na-MMT, smallest for multivalent counter-ions	Absorption of ammonia, proteins, dyes and other polar, aromatic and ionic compounds

These hydrophobic clay minerals have gained much interest because of their wide applications as adsorbents of organic pollutants (Stockmeyer, 1991, Ma and Zhu, 2007, Theng et al., 2008), as fillers in the preparation of clay-based polymer nanocomposites (Sinha Ray and Okamoto, 2003), and as precursors in the synthesis of mesoporous substances (Ishii et al., 2005).
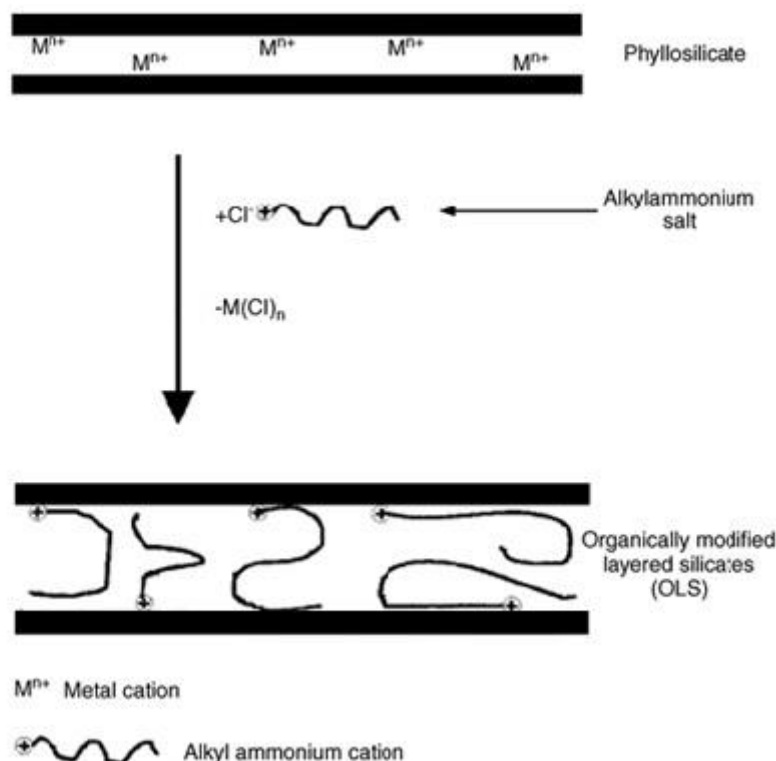
Figure 6: Schematic demonstration of clay organic modification. (Zanetti et al., 2000) Copyright 2000, Wiley-VCH Verlag GmbH & Co. KGaA.

2.1.3. Organically Modified Nano-Clays

'Organo-clays' are clays that have been modified with organic surfactants with different CEC and configuration (He et al., 2010, Janek and Lagaly, 2003). Different CEC in clays is because of the chemical composition which varies from one deposit to another. This variation arises from isomorphous substitution (e.g., Mg^{2+} for Al^{3+} in the octahedral sheet and/or Al^{3+} for Si^{4+} the tetrahedral

sheet) in the MMT layer. The resultant deficiency in positive layer charge is compensated by the adsorption of Na^+ or Ca^{2+} ions in the interlayer space.

The use of clays as such greatly limits the class of miscible polymers only to hydrophilic ones, mainly poly(ethylene oxide) and poly(vinyl alcohol). To overcome this restriction, the silicate surface is modified by exchanging the cations initially present in the interlayer with organic cationic surfactants, mainly including primary, secondary, tertiary and quaternary alkylammonium or phosphonium cations which contain various substituents (Figure 6). At least one of these substituents must be a long carbon chain of 12 carbon atoms or more, in order to make the clay mineral compatible with the polymer (Smith and Galan, 1995, Zhu et al., 1998, Wang et al., 2004, Yílmaz and Yapar, 2004).

The arrangement of the alkyl chains within the interlayers is highly dependent on the size of the chain as well as the number of chains (Lagaly, 1981, Heinz et al., 2007, Zhu et al., 2007). Figure 7 shows the interlayer arrangements of alkyl long-chains changing with the chain length.

The organic cations lower the surface energy of the inorganic host, improving the wetting property with the polymer matrix and result in larger interlayer spacing (swelling). Furthermore, their long aliphatic tails, attached with their cationic head via coulombic interactions to the surface of the negatively charged silicates, result in a larger interlayer spacing (Beyer, 2002, Lebaron et al., 1999, Zeng et al., 2005, Zanetti et al., 2000, Ke and Stroeve, 2005, Kiliaris and Papaspyrides, 2010). The organo-clays prepared, however, are structurally different under similar experimental conditions even with the same surfactant being used (Lagaly, 1981, Lee and Kim, 2002, Xi et al., 2005, He et al., 2006, Zidelkheir and Abdelgoad, 2008). This recommends that the structure and

properties of the resultant organoclays are affected by both the surfactant type and clay mineral used.

He *et al.* (He et al., 2010) reported that MMT with different CEC were modified using surfactants with different carbon chain lengths and numbers. They found that the maximum basal spacing is independent of the CEC when the same surfactant was used. However, the loading of surfactant was highly depended on the CEC. Also the maximum basal spacing of MMT modified with the double alkyl carbon chain surfactant was higher than the single ones.
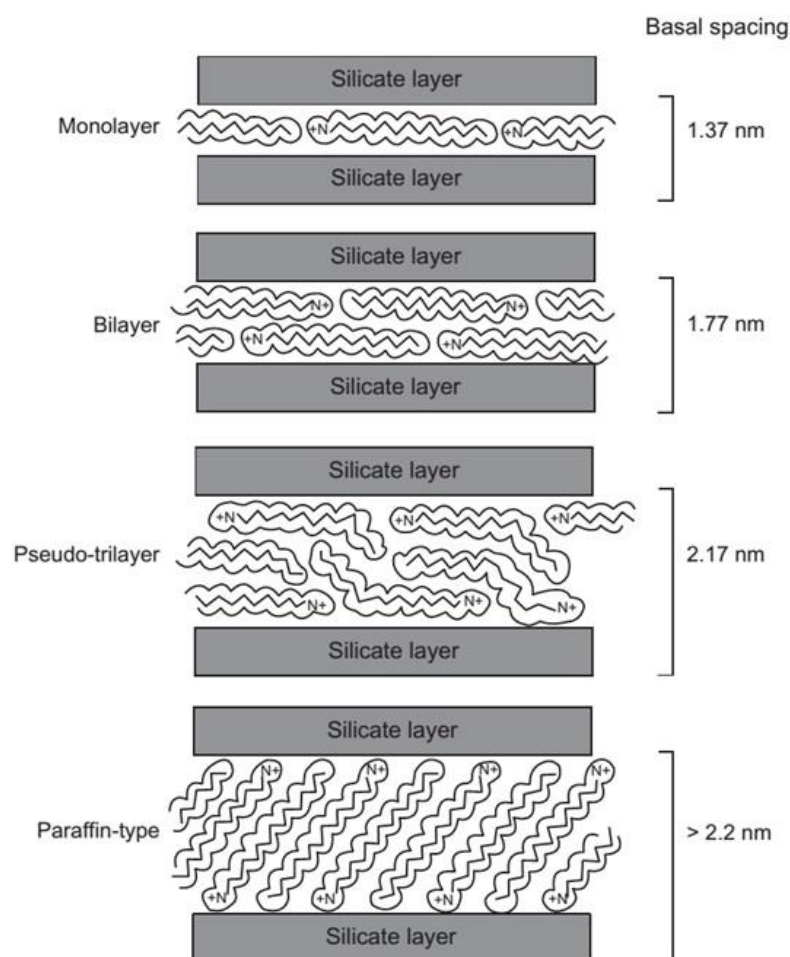
Figure 7: Possible arrangements of long-chain alkylammonium ions in the interlayer space of montmorillonite. The basal spacing of the different organoclays is indicated. From (Theng et al., 2008), based on diagrams by (Lagaly, 2006, Jaynes and Boyd, 1991)

2.1.3.1. Exfoliation

A text book (Utracki, 2004) defines the exfoliated layered material as "individual platelets (of an intercalated layered material) dispersed in a carrier material or a matrix polymer with the distance between them > 8.8 nm. The platelets can be oriented, forming short stacks or tactoids or they can be randomly dispersed in the medium."

Organoclays are well-known modifiers for rheological properties (Jones, 1983b). They are extensively used to modify the rheological properties of organic systems such as paints and greases. They can acts as thickeners and thixotropic agents. These properties depend on the exfoliation of the clay mineral particles and three dimensional assemblies into meso-scale card-house structures. A suitable chemical activator is used as a carrier for water which migrates in between the hydroxyl groups on adjacent clay particle edges. It forms hydrogen bonding between the hydroxyl groups assisting to develop and stabilize the gel structure. Application of high shear rates or prolonged action of lower shear forces causes progressive parallel alignment of the platelets leading to the observation of noticeable shear thinning (Wagener and Reisinger, 2003b). Hence, it was proposed that the intensity of the shear thinning effect can be a tool to characterize the degree of exfoliation of clay mineral particles in a polymer matrix (Massinga Jr et al., 2010, Wagener and Reisinger, 2003b) using similar wax melts or oils (Wang et al., 2008).

2.1.3.1.1. Mechanism of exfoliation of nanoclays

The clay particles present a very high aspect ratio of width/thickness, in the order of 10–1000. For very low concentrations of particles, the total interface between polymer and layered silicates is much greater than that in conventional composites. Depending on the strength of the interfacial interaction, four types

of dispersion of layered silicates in a polymer matrix (see Figure 8) (Utracki, 2004) :

    (A) Conventional dispersion of non-intercalated clay particles with the basic dry structure,

    (B) intercalated and flocculated form where the interlayer spacing $d_{001} < 8.8$ nm, and

    (C or D) exfoliated structures where $d_{001} > 8.8$ nm with the individual platelets either ordered (because of stress field or concentration effects) or not, respectively.

A: Conventional composite

B: Intercalated nanocomposite

C: Ordered exfoliated nanocomposite

D: Disordered exfoliated nanocomposite
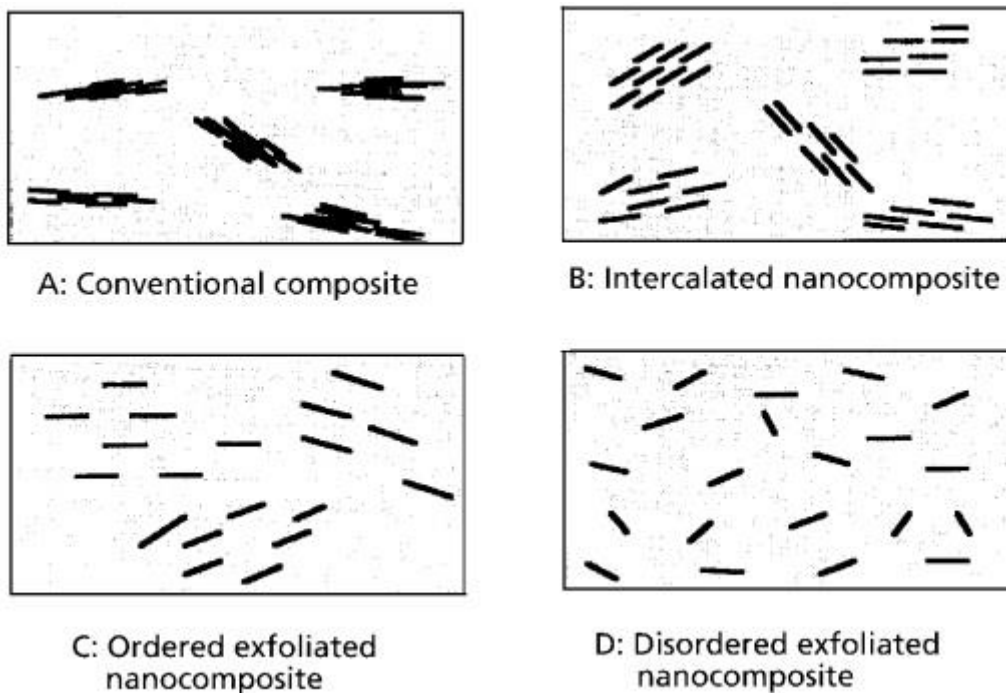
Figure 8: Four types of clay platelet dispersions in a polymeric matrix (Utracki, 2004)

In aqueous suspension the clay platelets may form more complex structures (see Figure 9). The platelet association (flocculation) may occur by face-to-face (FF), face-to-edge (FE) or edge-to-edge (EE) interactions (Qian et al., 2000) with each clay structure resulting in a different set of suspension properties.

(Okamoto et al., 2001) reported formation of a 'house of cards' structure in polypropylene (PP)/clay nanocomposite melt under extensional flow. The authors considered that high strain hardening and rheopectic effects originate from the perpendicular alignment of the silicate layers to the stretching direction. When the stress vanishes, the platelets form the complex structures.
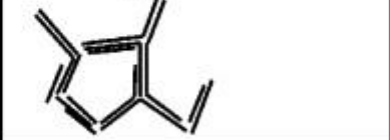
Figure 9: Structures encountered in clay suspensions (Qian et al., 2000)

The key objective for the successful development of polymer nanocomposites is to achieve complete exfoliation of the layered silicate in the polymer matrix. The three most common methods that are used for the synthesis of polymer-nanocomposites are:

(1) Intercalation in a suitable monomer and subsequent in situ polymerisation that leads to exfoliation.

(2) Intercalation of polymer from solution and exfoliation.

(3) Polymer melt-blending intercalation and exfoliation.

2.1.3.2. Properties

The nanocomposites have become an area of intensive research activity within both the scientific and engineering communities. They exhibit outstanding physical and mechanical properties different from their traditional polymer composites filled with micro-sized additives such as better thermal stability, high heat distortion temperature, superior gas/liquid barrier properties (permeability, flammability), and high specific stiffness (or strength) at low concentrations of clay (< 5 wt.%) in a range of polymer matrices (polyimide, polyester, polycaprolactone, poly(butylenes succinate), poly(urethane urea) and poly(vinyl alcohol etc.,) (Yano et al., 1997, Koo et al., 2003, Ray et al., 2003, Bharadwaj et al., 2002, Strawhecker and Manias, 2000). It is generally believed that the improvements of their barrier and other mechanical properties are mainly caused by the high aspect ratio (10 - 1000) or the large surface area of the exfoliated clay particles and the strong interfacial interaction between the silicate platelets and the polymer matrix (Yano et al., 1997, Koo et al., 2003, Ray et al., 2003, Bharadwaj et al., 2002, Strawhecker and Manias, 2000, Gersappe, 2002, Calvert, 1996, Giannelis, 1996).

The most important property driving the development of polymer nanocomposites is their high mechanical strength. The complete dispersion of clay nanolayers in a polymer enhances the number of available reinforcing elements that carry an applied load and deflect the evolving cracks. The coupling between the large surface area of the clay and the polymer matrix facilitates the stress transfer to the reinforcing phase allowing for the improvement of the tensile stress and toughness (Lebaron et al., 1999, Powell and Beall, 2006, Jordan et al., 2005).

The second major improvement of the nanocomposites is their enhanced barrier properties. The impermeable clay layers create a tortuous pathway for a

permeant traversing the nanocomposite. Theoretically, gas permeability through polymer films can be reduced by 50–500 times even with small loadings of nanoclays. The relevant research on polymer–clay nanocomposite concerns mostly highly volatile natural repellents in different product designs (Choudalakis and Gotsis, 2009).

2.1.4. Permeability of Polymer nanocomposites

Modified MMT clays are the most commonly used layered silicates for the preparation of polymer nano-composites. The single sheet thickness is about 1 nm and the lateral dimensions can be in the micron range. When delaminated and dispersed in a polymer matrix it provides a structure with an extensive filler-matrix contact surface. The clay sheets are relatively stiff and impermeable to molecular diffusion. With a low concentration of layered silicates (~ 5 vol %) in a polymer matrix, the remarkable reduction in gas/liquid permeability, one of the typical barrier properties, has been reported by many authors (Lan et al., 1994, Messersmith and Giannelis, 1994, Yano et al., 1997, Strawhecker and Manias, 2000, Xu et al., 2001, Bharadwaj et al., 2002, Ray et al., 2003, Kim et al., 2005a, Lai and Kim, 2005). In most theoretical papers the polymer nanocomposites is considered to be consisting of two phases: one is a permeable phase (polymer matrix) and another is a non-permeable phase (dispersed nanoclay particles). The mass transport mechanism of gas/liquid in a nanoclay filled polymer is similar to that in a semi-crystalline polymer. Three main factors that affect the permeability of a nanocomposite are: the volume fraction of the organoclay particles; their orientation with respect to the diffusion direction; and their aspect ratio.

It is generally accepted that the transport mechanism of gas/liquid within the polymer matrix can be described using three parameters: permeability, solubility and diffusion coefficients (Sorrentino et al., 2006) where the

permeability is often described as the product of diffusion coefficient and solubility in a steady state condition (Hansen, 2000). Fick's second law of diffusion is generally applied to explain the transport mechanism since the matrix maintains the same properties and characteristics as compared to the neat polymer (Beek, 1999, Welty, 1984). A decrease of the solubility is, therefore, expected in the nanocomposite owing to the reduced polymer matrix volume, along with a decrease in diffusion due to a more tortuous path for the diffusing molecules.

According to Fick's linear diffusion law, the permeability P_p can be expressed by

$$P_p = j\, d/\Delta p \qquad\qquad (2)$$

where j is the permeant flux and Δp is the pressure difference across the film of thickness d.

2.1.4.1. *Tortuous path model*

If it is considered that silicate platelets are impenetrable to the permeating molecules. Thus the molecule must go round these sheets. This results in a very long tortuous path. Let's only focus on geometric factors of clay particles ignoring the influence of the silicate platelets on a polymer matrix such as the mobility of polymer chains. Then, the major factors influencing the barrier property of polymer-clay nanocomposites are mainly determined by the extent of exfoliation and/or intercalation and the condition of dispersion of silicate platelets in the matrix, such as aspect ratio L/W (L and W are the length and thickness of silicate platelets, respectively), orientation θ, the dispersion spacing ξ between two platelets and volume fraction ϕ. On the bases of the dimensional analysis, the permeability P_c, of gas/liquid molecules in a polymer-clay nanocomposite is given by (Tjong and Mai, Lu and Mai, 2007):

$$P_c = P_p f\left(L/W,\, L/\xi,\, \phi,\, \theta, ...\right) \qquad\qquad (3)$$

where P_p is the permeability coefficient of the polymer without the addition of clay, and *f* is a function of several dimensionless parameters such as *L/W*, *L/ξ*, ϕ, *θ*, etc. Here, it is clear to see that *L/W* determines the degree of exfoliation or intercalation, and *L/ξ* represents the extent of dispersion of clay platelets in the polymer matrix.

Based on the tortuosity argument, Nielsen (1967) (L.E., 1967) proposed the tortuous path model to explain the effect of platy fillers on relative barrier performance. This model has been widely used to explain the permeability behaviour of polymer-clay nanocomposites. Let us consider a model where clay particles are exfoliated and uniformly staggered along the orientation direction ($\theta = 0°$) in a polymer film (see Figure 10). The tortuous factor τ is defined by:

$$\tau = \frac{detour\ distance\ a\ molecule\ gets\ through\ film}{thickness\ of\ film} = 1 + \frac{1}{2}\frac{L}{W}\phi \qquad (4)$$
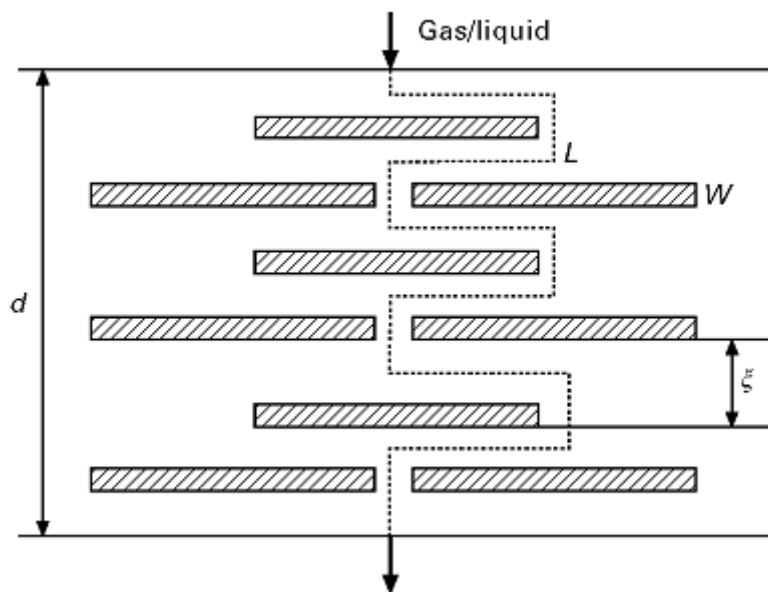
Figure 10: Schematic representation of the tortuous path of a gas/liquid molecule passing through a polymer filled with silicate platelets.

Then, the relative permeability, $P_r = P_c/P_p$, in the polymer film can be expressed by:

$$P_r = \frac{1 - \phi}{\tau} \approx \left(1 + \frac{1}{2}\frac{L}{W}\phi\right)^{-1} \tag{5}$$

where $1 - \phi \to 1$, since the volume fraction $\phi \ll 1$ in most polymer-clay nanocomposites. Conversely, if the silicate platelets are oriented perpendicular to the film surface, the relative permeability P_r should be replaced by:

$$P_r = \frac{1 - \phi}{\tau} \approx \left(1 + \frac{1}{2}\frac{W}{L}\phi\right)^{-1} \tag{6}$$

Clearly, the relative permeability P_r is dependent on the aspect ratio (or degree of exfoliation) of clay platelets (*L/W* or *W/L*) and their orientation (θ). Now, to consider the influence of orientations on permeability, Bharadwaj (Bharadwaj, 2001) extended the Nielsen model by introducing an order parameter S that was defined as $S = 1/2\,(3cos^2\theta - 1)$, where $-1/2 < S \leq 1$ (de Gennes, 1974). As shown in Figure 11, $S = 1$ ($\theta = 0°$) indicates the case of perfect alignment, and in the case of $S = -1/2$ ($0 = 90°$), there is almost no barrier role for the clay platelets to the diffusion of gas/liquid molecules in polymers. $S = 0$ ($<\theta> = 54.74°$) agrees to the random orientation of exfoliated clay platelets. Hence, the relative permeability P_r of polymer-clay nanocomposites can be rewritten as:

$$P_r \approx \left(1 + \frac{2S + 1}{6}\frac{L}{W}\phi\right)^{-1} \tag{7}$$

Comparison of Equation (7) with Equation (5) shows the influence of orientations of silicate platelets on permeability is equivalent to a decrease of their effective aspect ratios. Here, it is worth noting that the exfoliated silicate platelets are usually randomly dispersed within the polymer matrix. However, the potential effect of silicate platelets on permeability along a third direction was ignored in such a two-dimensional model.

In practice permeability improvement is limited owing to the fact that, at higher clay levels exfoliation is limited, probably owing to a collapse mechanism

(Osman et al., 2004). For example, Osman *et al.* (Osman et al., 2004) found that permeability improvement levels of at ca. 3% nano clay loading. Their relative transmission rate was only ca. 60%.
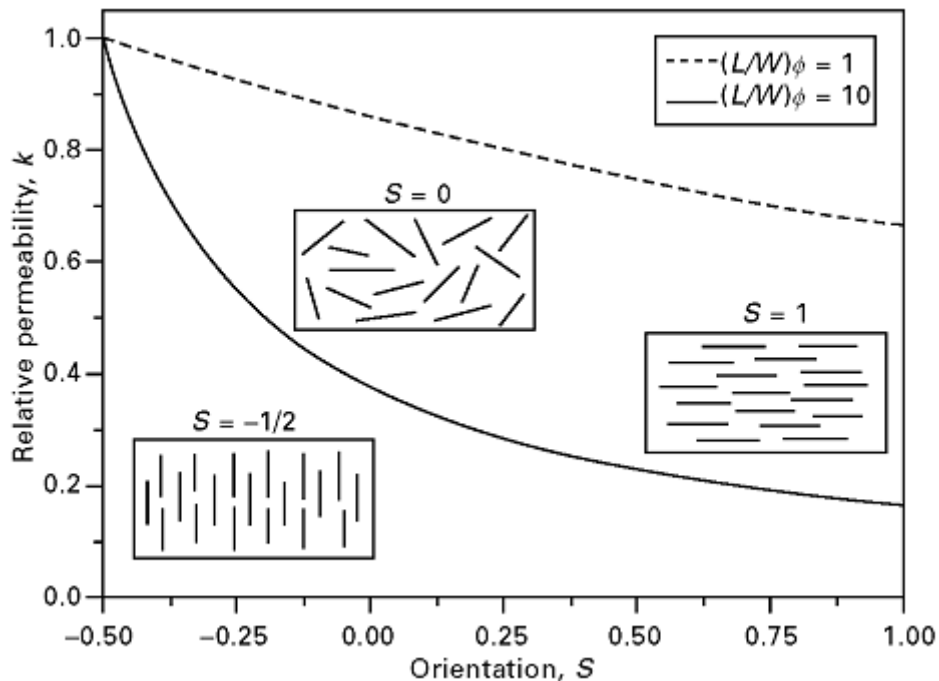
Figure 11: Influence of platelet orientation on the relative permeability in polymer-clay nanocomposites, where insets illustrate three typical distributions at $S = -1/2$, 0 and 1 (Bharadwaj, 2001).

2.2. Citronellal

Citronellal 3,7-dimethyloct-6-en-1-al ($C_{10}H_{18}O$) is one of the major components of citronella oil (around 35 to 40%) giving its distinctive lemon scent (Licciardello et al., 2013b). It is a natural aroma compound which has a tendency to repel mosquitoes. Figure 12 shows the chemical structure of the citronellal.
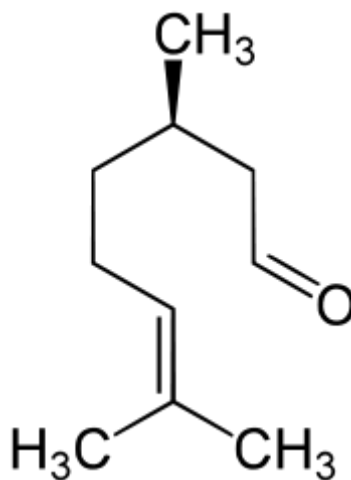
Figure 12 : Chemical structure of citronellal (3,7-dimethyloct-6-en-1-al)

Various researchers have tested the repellency of citronellal. Kim et al. (KIM et al., 2005b) tested the repellent efficacy of citronellal and citronella oil. It was found that citronellal has a percentage repellency of 78% compared to citronella oil of 86% at same levels of dosage. Another study (Cockcroft et al., 1998) shows that repellent property of citronellal is as effective as DEET, only if it is used at higher concentrations. Similar work was conducted by Licciardello et al. (Licciardello et al., 2013c), where they tested the repellent efficacy of essential oils in food packaging materials. Using the organic coating containing essential oils on corona treated polypropylene; they claim that the repellent efficacy of essential oils can last for more than 4 months.

Charara et al. (Charara et al., 1992) tested the absorption of essential oils in various polymeric packaging materials. They found that polymers with large amorphous regions absorbed more essential oils than the ones with higher crystallinity. They also found that aldehydes like citronellal cannot be absorbed at large quantities (<10%) by polyolefin materials.

Licciardello et al. (Licciardello et al., 2013a) studied the diffusional behaviour of essential oils components in packaging materials. They found that diffusion

coefficient is highly depended on the initial concentrations of essential oil components as well as their M_w and polarity. Comparing the M_w of two essential oil components, higher M_w showed lower diffusion coefficient across polypropylene film and vice versa. Also components with similar M_w but different polarities showed an effect on diffusion coefficient. Higher polarity component showed faster diffusion than the lower polarity one. It is true for non-polar polymeric materials. For polar polymeric materials, higher polarity of essential oil components would diffuse slower than the lower polarity ones (López et al., 2007).

2.3. Microporous Polymers

Different techniques have been used to form microporous polymer structure, some of which are as follows:

- Solvent induced phase separation (SIPS) (Abedin et al., 2014)
- Non-Solvent induced phase separation (NIPS) (Ishigami et al., 2014)
- Thermally induced phase separation (TIPS)
- Thermally assisted evaporation phase separation (TAEPS) (Hellman et al., 2004)

In all the above mentioned techniques, TIPS technique has been used widely in polymers due to the simplicity of the setup and fewer factors affecting the microporous structure formation.

2.3.1. Thermally induced phase separation technique

Microporous polymers have been researched extensively and they have also found numerous practical applications in chemical technology (Ulbricht, 2006). The TIPS process was introduced by Castro (Castro, 1981) and it is one of the leading techniques for the preparation of microporous polymer structures (Lloyd et al., 1990b). The key benefit of the TIPS process is that there are fewer factors

influencing the microporous structure formation (van de Witte et al., 1996) compared to NIPS method. Many different forms like films, blocks, intricate shapes, etc. can be made from thermoplastic polymers, such as, polyolefins. They are relatively homogeneous, three-dimensional cellular structure where the cells are connected by small pores. Polyolefin microporous structures have received considerable attention owing to their good thermal and solvent resistance as well as their low cost (Caneba and Soong, 1985, Hiatt et al., 1985, Lloyd et al., 1990a, Tsai and Torkelson, 1990, Lloyd et al., 1991, Mehta et al., 1995, Kim et al., 1995, Matsuyama et al., 1999, Matsuyama et al., 1998, Castro, 1981). Practical examples include use in haemodialysis processes, artificial kidneys (Ulbricht, 2006), the removal of bacteria and viruses (Qiu and Matsuyama, 2010), treatment of waste water (Yave et al., 2005), oil-water separation (Funk and Lloyd, 2008), use in batteries (Vanegas et al., 2009, Cui et al., 2008), gas separation (Funk and Lloyd, 2008), etc. Adjusting TIPS parameters, such as types of polymers, solvent to polymer ratio, quenching temperature can be adjusted to obtained materials with distinctive morphologies suitable for various applications (de Lima and Felisberti, 2009, Luo et al., 2008).

Li *et al*. reported the formation of microporous polyethylene (PE) membrane via the TIPS process using low-density polyethylene (LDPE) and high-density polyethylene (HDPE) (Li et al., 1995). The density effect was later investigated where the HDPE membrane showed about five times higher water permeability than the LDPE membrane because of the larger pore size and the higher porosity at the outer membrane surface (Matsuyama et al., 2004).

The TIPS process involves heating a polymer and a diluent to a sufficiently high temperature for melt-blending the components into a homogenous phase. The diluent is usually a low molecular weight, high-boiling point solvent in which

the polymer is not soluble at room temperature, but solubilizes the polymer at higher temperatures. A typical temperature composition phase diagram for a binary polymer–solvent system with an upper critical solution temperature is presented in Figure 16. There are two curves, binodal and spinodal, that represents the thermodynamic equilibrium of liquid–liquid (L-L) de-mixing or phase separation. Area above the curves represents the polymer solution to be homogenous. The maximum point, at which both the binodal and the spinodal curves merge, is the critical point of the system. The area under the spinodal curve is thermodynamically unstable region. The region located in the zone between the binodal and spinodal curves on both sides is the metastable region.

The phase separation process in the metastable region proceeds according to a nucleation and growth mechanism. The resultant structure depends upon the polymer concentration to be lower or higher than the critical point concentration (Nunes and Inoue, 1996, Sperling, 2005). Droplets of the minority phase form spontaneously. If they are large enough they become stable nuclei and continue to grow. They keep growing until phase separation is complete. Typically, if the polymer constitutes the minority phase, this will result in loose polymer powder particles suspended in the diluent. At higher concentrations the particles may grow and impinge on one another. This results in the coalescence of phase-separated droplets. Dispersions with small droplets have a high interfacial surface area. So these systems always tend to continuously decrease, i.e. minimize the interfacial free energy associated with the interfacial area. In some cases it is possible for small droplets to dissolve at the expense of larger ones growing. This effect is induced by a differential interfacial tension exerted between the two phase separated domains. If the oil phase is the minority phase, the coarsening process results in pore size enlargement via Ostwald ripening, coalescence (Mooney et al., 1996, Lo et al., 1996). However, it tends to generate closed pores; thus, it is important to optimize various parameters to

achieve an interconnected and open macroporous open structure (Song and Torkelson, 1995).

On the other hand, if the homogenous solution is cooled fast enough to low enough temperatures, spinodal decomposition is induced. It is a process whereby spatial concentration differences are amplified during phase separation. The mixture separates into co-continuous polymer-rich and polymer-poor phases (Vandeweerdt et al., 1991, Williams and Moore, 1987). Upon further cooling, the polymer matrix phase crystallizes (i.e. solidifies) and locks-in the solid matrix structure. Subsequently the diluent can be extracted (Castro, 1981). This results in a well-interconnected co-continuous microporous structure.

2.3.2. Thermodynamic description of binary mixtures

Mixtures are systems consisting of two or more different chemical species. Binary mixtures consist of only two different species. An example of a binary mixture is a blend of polystyrene and polybutadiene. If the mixture is uniform and all components of the mixture are intermixed on a molecular scale, the mixture is called homogeneous. An example of a homogeneous mixture is a polymer solution in a good solvent. If the mixture consists of several different phases (regions with different compositions), it is called heterogeneous. An example of a heterogeneous mixture is that of oil and water. Whether an equilibrium state of a given mixture is homogeneous or heterogeneous is determined by the composition dependence of the entropy and energy changes on mixing. Entropy always favours mixing, but energetic interactions between species can either promote or inhibit mixing (Lovell, 2011).

There are three types of binary mixtures which are described in detail in many textbooks (Lovell, 2011, Rubinstein and Colby, 2003, Валас, 1985), as follows:

- Ideal mixtures

- Polymer solutions
- Polymer blends

Ideal mixtures are the solutions in which the molecules of both the components are identical in size and intermolecular attractions of like and unlike molecules are the same. The latter gives rise to the condition where there are no changes in the entropies associated with individual molecules (rotational, vibrational and translational) of the mixed components. Furthermore the mixing proceeds athermally, i.e. the enthalpy of mixing is zero ($\Delta H_{mix}= 0$). However, ideal mixing does lead to a positive configurational entropy change (ΔS_{mix}). This is the result of an increase in the number of distinguishable spatial arrangements of the molecules. In order to derive an equation for change in Gibb's free energy (ΔG_{mix}) for the ideal mixture, it is assumed that the molecules are placed randomly into cells which are of molecular size and arranged in the form of a three dimensional lattice (represented in two dimensions) for cubic cells as shown in Figure 13.
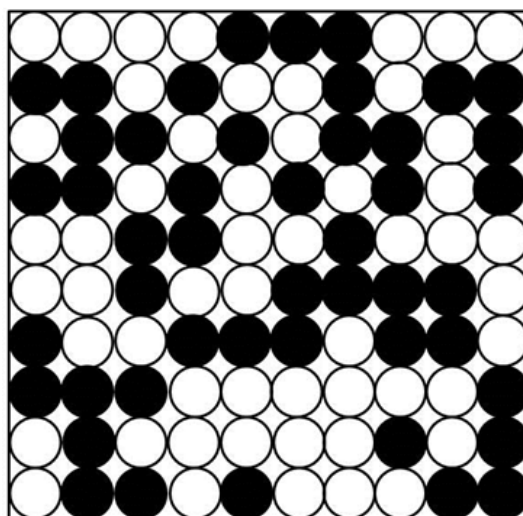
Figure 13: Binary mixture of a regular / ideal mixture

Therefore, for the formation of an ideal mixture, the change in Gibb's free energy can be given as,

$$\Delta G_{mix} = RT[n_1 ln X_1 + n_2 ln X_2] \qquad (8)$$

where, R is the universal gas constant, T is the absolute temperature, n_1 and n_2 are the numbers of moles and X_1 and X_2 are the mole fractions of the components.

Equation (8) gives rise to the fundamental basis for thermodynamics of ideal mixtures, however, it does not fulfil the conditions for non-ideal mixtures where small molecules are mixed with relatively large molecules (e.g. in polymer solutions). Therefore, Flory (Flory, 1941) and Huggins (Huggins, 1941) independently proposed a modified lattice model in 1941 where the large differences in molecular sizes between solvent and polymer molecules as well as intermolecular attractions were taken into account.

Polymer Solutions are the mixtures in which long-chain polymer molecules are mixed with relatively small solvent molecules. In order to predict ΔG_{mix} for the formation of polymer solutions, according to Flory-Huggins (F-H) theory, it is considered that the polymer molecules (denoted by a subscript 2) are the chains of segments in which each segment is equal in size to a solvent molecule (denoted by a subscript 1). The total number of segments 'x' in the chain actually describes the size of a polymer molecule and can be understood as the ratio of the molar volume of polymer to the molar volume of solvent. Therefore, it is possible to place solvent molecules and polymer molecules in a three-dimensional lattice comprising of identical cells and each cell is equal to the size of a solvent molecule and occupied by either a molecule or a chain segment. Each polymer molecule is placed in the lattice so that its chain segments consecutively placed in vacant neighbouring cells. Thus they occupy a continuous sequence of x cells as shown in Figure 14. The total number of cells

is given by $N = N_1 + xN_2$, i.e. it is the sum of all the solvent molecules and polymer segments present.
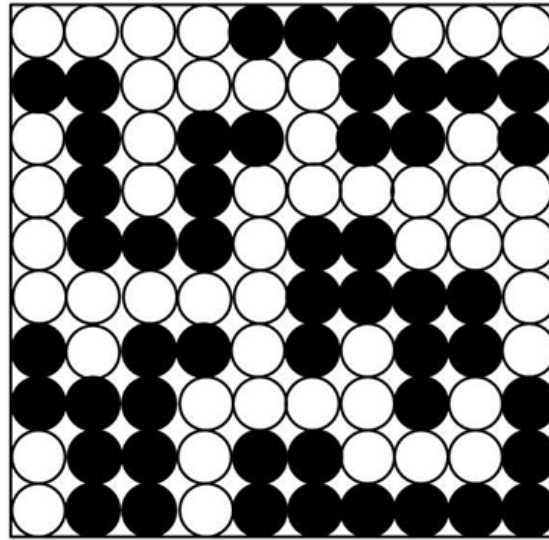
Figure 14: Binary mixture of a polymer solution of five black 10-ball chains

Since each molecule in a polymer can adopt many different conformations, which are, distinguishable spatial arrangements of the chain of segments, the above setup defines the condition for change in entropy ΔS_{mix} when ΔH_{mix} is NOT equal to zero. Therefore, ΔS_{mix} and ΔH_{mix}, according to F-H theory can be expressed as

$$\Delta S_{mix} = -R[n_1 ln\phi_1 + n_2 ln\phi_2] \tag{9}$$

and,

$$\Delta H_{mix} = RTn_1\phi_2\chi \tag{10}$$

where ϕ_1 and ϕ_2 are the volume fractions of solvent and polymer, respectively, and are given by $\phi_1 = N_1/(N_1 + xN_2)$ and $\phi_2 = x N_2/(N_1 + xN_2)$. This expression can be written in terms of number of moles by simply replacing number of molecules N_1 and N_2 with n_1 and n_2 ($n_1 = N_1/N_A$ and $n_2 = N_2/N_A$) respectively. χ is the F-H polymer-solvent interaction parameter and is a temperature-dependent dimensionless quantity that can be expressed more simply in the form

$$\chi = a + b/T \tag{11}$$

where a and b/T are the entropic and enthalpic components of χ.

Since Gibb's free energy is expressed as,

$$\Delta G_{mix} = \Delta H_{mix} - T\Delta S_{mix} \tag{12}$$

Therefore, by substituting Equation (9) and (10) in Equation (12), it can be re-written as,

$$\Delta G_{mix} = RT[n_1 ln\phi_1 + n_2 \ln \phi_2 + n_1\phi_2\chi] \tag{13}$$

This is the F-H equation for the Gibb's free energy of mixing per lattice site. For polymer solutions Equation (13) can be re-written in terms of Gibb's free energy of mixing per mole of lattice sites (or segments) as (Please see Appendix 1 for derivation),

$$\Delta G_{mix} = RT\left[(1 - \phi_2)\ln(1 - \phi_2) + \frac{\phi_2}{x}\ln\phi_2 + \chi(1 - \phi_2)\phi_2\right] \tag{14}$$

2.3.3. Phase-Separation behaviour of polymer solutions

In Equation (13), the first two terms represents the entropy of mixing. They make a negative contribution to the Gibbs free energy promoting thereby miscibility. The last term represents the enthalpy of mixing. In the F-H theory it is always positive promoting immiscibility. The temperature and interaction parameter χ actually defines the balance between the two contributions and describes the phase separation of the polymer solution, if any. Therefore, a series of curves for ΔG_{mix} with ϕ_2 can be plotted at different temperatures which can have one of two general forms as shown in Figure 15. For the temperature at which the curve only shows one minimum point, it describes that the solution is homogenous at all the concentrations of ϕ_2. If point A is considered at temperature T_{1b}, it is easy to show that the Gibbs free energy change associated with the phase separation phenomena is given by the difference between (i) the value of ΔG_{mix} corresponding to the point of intersection of the tie-line (joining points a' and a'') with the vertical $\phi_2 = \phi_{2A}$

line, and (ii) the value of ΔG_{mix} on the curve at A. Undoubtedly this difference is positive for all the points on the curve which favours the existence of a single homogenous phase for all ϕ_2.

For the temperature at which the curve shows two minimum points, the situation is more complex since the solution can have stable, unstable and metastable state depending on the position of the concentration of ϕ_2 on the curve. Consider phase separation at point A, all the compositions in the range of $0 < \phi_2 < \phi'_{2b}$ are stable and therefore, correspond to homogenous solution with no phase separation. Similarly, all the compositions in the range of $\phi''_{2b} < \phi_2 < 1$ are also stable. Now consider the phase separation at point D, the vertical line from point D intersect tie lines joining two points (d' and d'') *below* the curve. Thus the ΔG_{mix} at point D is negative and so the homogenous solution is unstable and phase separation takes place until the system reaches a stable state where the two co-existing phases acquire the binodal compositions ϕ'_{2b} and ϕ''_{2b}. Within the range of $\phi'_{2sp} < \phi_2 < \phi''_{2sp}$, all the homogenous solutions are unstable and separate into two phases, where ϕ'_{2sp} and ϕ''_{2sp} are the points of inflection on the curve defining spinodal compositions.
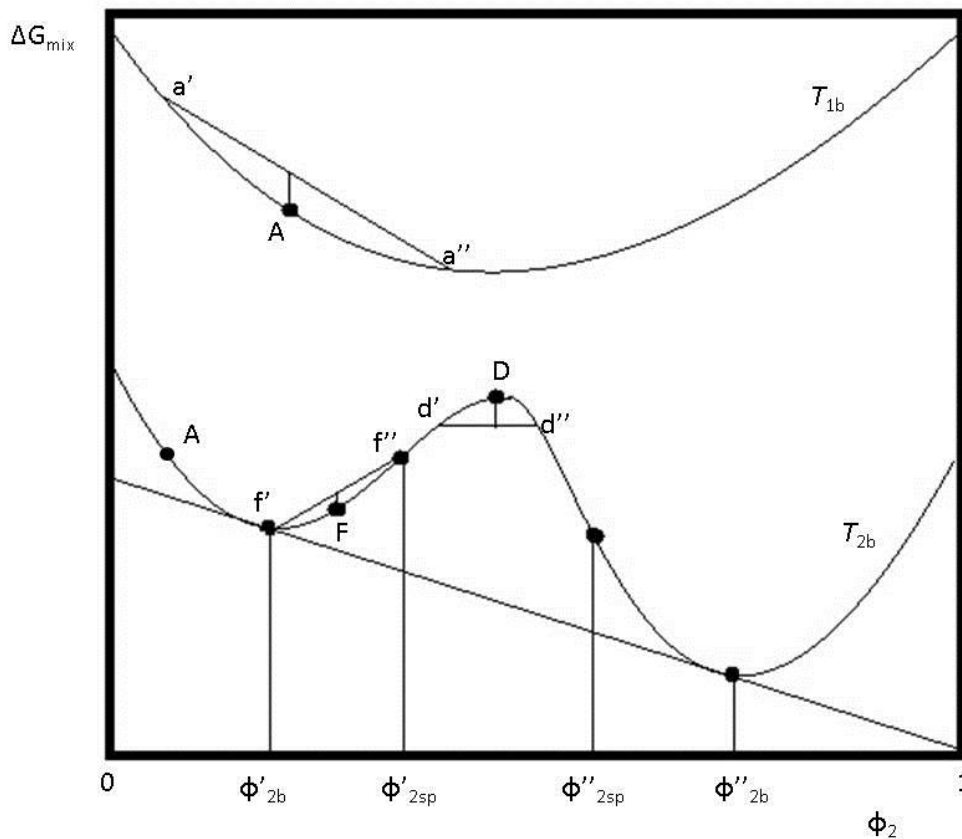
Figure 15: Schematic illustration of the variation of ΔG_{mix} with $\boldsymbol{\phi_2}$ and temperature T shows, for the two types of ΔG_{mix} vs $\boldsymbol{\phi_2}$ curve, the constructions used to identify regions of $\boldsymbol{\phi_2}$ where an initially homogenous solution with stable, unstable, or metastable towards phase separation

Lastly, consider the phase separation at point F on the curve, the homogenous solution is metastable and phase separation takes place into two binodal compositions provided an energy barrier must be overcome. This is because the initial stage of phase separation gives rise to an increase in the Gibb's free energy. This is valid for all the compositions in the ranges $\phi'_{2b} < \phi_2 < \phi'_{2sp}$ and $\phi''_{2sp} < \phi_2 < \phi''_{2b}$.

The general condition for equilibrium established across the co-existing phase, that is, the chemical potential of the components are about the same in both co-

existing phases. This condition is written as the difference in chemical potential and is directly related to ΔG_{mix} as,

$$\mu_1 - \mu_1^0 = \mu_1'' - \mu_1^0 \qquad (15)$$

$$\mu_2 - \mu_2^0 = \mu_2'' - \mu_2^0 \qquad (16)$$

Their values can be determined by plotting a common tangent between the two minima on the curve vertically intersecting at $\phi_2=0$ and $\phi_2=1$ lines, respectively (Lovell, 2011).
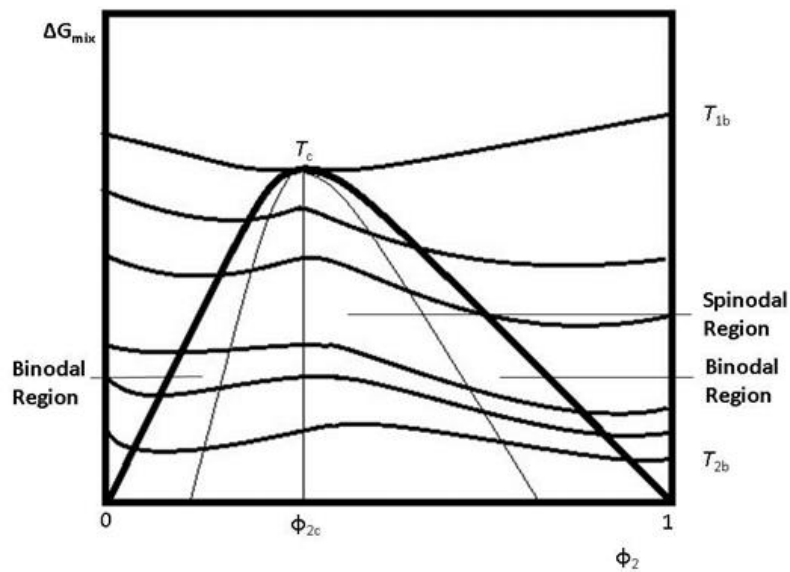
Figure 16: Schematic illustration of the variation of ΔG_{mix} with $\boldsymbol{\phi_2}$ at different temperatures T shows how the shape of the curves changes with T. Binodal and Spinodal points are joined together at the two minima and inflection points respectively to form the UCST phase diagram.

The presence of two minima in the plot of ΔG_{mix} with ϕ_2 (i.e. phase separation) is due to contact interaction χ and as a result, enthalpy of mixing ΔH_{mix} is nonzero, which cause ΔG_{mix} to increase. This effect reduces as the temperature increases from T_{2b} towards T_{1b} in Figure 16 and hence the binodal and spinodal points get closer to each other until reach at a critical temperature T_c

corresponding to critical concertration ϕ_{2c}. In Figure 16, the curves are drawn by joining binodal and spinodal points as a function of temperature are known as the binodal and spinodal respectively.

Mostly, for the polymer solutions, the value of χ decreases as temperature increases (Equation (11)). This result in a solution to be homogenous in all proportions above the critical temperature and is known as the upper critical solution temperature (UCST). Figure 16 is an example of UCST. And if the value of χ increases as temperature increases then the solution is homogenous (or miscible) below the critical temperature and is known as the lower critical solution temperature (LCST). An example of LCST is simply the reverse of Figure 16.

Since the spinodal compositions take place at points of inflection, they can be located by taking the derivative of Equation (14) and equating it to zero.

$$(\partial^2 \Delta G_{mix}/\partial \phi_2^2)^{\alpha,\beta} = 0 \tag{17}$$

Since, for both UCST and LCST, the critical temperature meets at the turning point for binodal and spinodal, therefore, critical concentration can be located by applying the condition on Equation (14) as,

$$(\partial^3 \Delta G_{mix}/\partial \phi_2^3)^{\alpha,\beta} = 0 \tag{18}$$

3   First Concept

3.1   Introduction

In recent years, polymer nanocomposites have gained popularity due to their enhanced mechanical, chemical and barrier properties. (Xu et al., 2006) reported that by introducing nanoclays into polymer, intercalated and/or incomplete exfoliated structures and dispersed tactoids with several layers can effectively enhance the barrier properties by increasing the path length of the volatile through the matrix. This can be achieved by using a polymer which is highly amorphous and contains exfoliated clay nanoparticles. Clays are minerals comprising thin two-dimensional sheets. Via appropriate organic modification it is possible to facilitate exfoliation of these sheets inside the polymer matrix. The individual clay sheets are impermeable to small molecules. This means that well-dispersed fully exfoliated clay sheets present diffusion barriers. The overall release rate of liquid actives via diffusion through such membranes rate is significantly reduced by the huge increase in the tortuosity of the diffusion path dictated by the presence of the dispersed clay sheets (Pavlidou and Papaspyrides, 2008). This concept is illustrated in Figure 17.
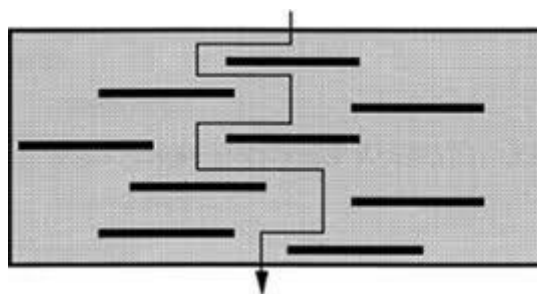
Figure 17: Incorporation of exfoliated and suitable oriented clay platelets reduces the permeability of a polymer film by increasing the effective diffusion path (tortuosity).

Unfortunately, clays are usually hydrophilic while polymers are oleophilic. Hence it is often not easy to coax clay sheets to exfoliate. Usually it is necessary to employ organo-modification techniques. In essence it entails replacing the

inorganic cations in the clay galleries with organic ones. The surfactant choice is crucial as it should be fully compatible with the matrix polymer otherwise exfoliation will not be favoured.

3.2 Experimental

3.2.1 Materials

Ethylene Vinyl Acetate copolymer (EVA) (Grade EV101; MFI 1.8 @190°C, 2.16 kg; density 0.940 g/cm^3; VA content 18%) was supplied by Affirm.

Linear low density polyethylene (LLDPE) (Grade HR 411: MFI 3.5 @190°C, 2.16 kg); density 0.939 g/cm^3; particle size: 90% < 600 μm) was supplied by Sasol Polymers. White Oil was manufactured by Savita Oil Technologies Limited, batch no : LD 589 12. Citronellal (3,7-dimethyloct-6-en-1-al), ethanol (97%), acetic acid and stearic acid were obtained from Merck Chemicals. Organically modified clay (Dellite 43B) was supplied by a local South African based company called Laviosa Chemicals. This clay is recommended by supplier to be used with polyolefins and EVA. It is organically modified with Dimethyl benzyl hydrogenated tallow ammonium (DMBHTA). The typical levels of use recommended by the supplier are in the range of $1 - 5\%$ based on total system weight.

3.2.2 Methods

Organoclays are well-known rheology modifiers and are widely used as thickeners and to control the thixotropic properties of organic systems such as paints and greases. This is due to their propensity for exfoliation and a three dimensional assembly into mesoscale card-house structures (Jones, 1983a). Water, carried in by a suitable chemical activator and migrates in between the hydroxyl groups on adjacent clay particle edges. It forms hydrogen bond bridges between the hydroxyl groups helping to develop and stabilize the gel

structure. Application of high shear rates or prolonged action of lower shear forces causes progressive parallel alignment of the platelets leading to the observation of pronounced shear thinning (Wagener and Reisinger, 2003a). In fact, it was proposed that the intensity of this effect can be used to characterize the degree of exfoliation of clay mineral particles in a polymer matrix (Massinga Jr et al., 2010, Wagener and Reisinger, 2003a) or in similar wax melts or oils (Wang et al., 2008).

Using the above concept, different experiments were carried out in order to determine the correct amount of activator that will minimize the amount organoclay necessary to form a three dimensional structure in the polymer. To do this, white oil was taken as model compound for the polymer. This was done as it is also an alkane-like material just like polyethylene. Furthermore it is a liquid at room temperature with a much lower viscosity than the polymer melt. Hence it was easier to compound. Different formulations were prepared with clay using hand mixing. The following are the results:

White oil:Clay – 50:50 – thick paste
White oil:Clay – 65:35 – Slurry followed with phase separation

Activator with an -OH functional group
From the above, it was concluded that there will be a need for an activator in order to achieve the single phase mixture of clay into white oil without any phase separation afterwards. Therefore, ethanol was chosen as an activator since it contains hydroxyl group (-OH) as it was reported (Marini et al., 2009) that polarity does improve the compatibility between the organoclay and the polymer matrix. Following are the results of different formulations:

White Oil:Clay:Ethanol – 65:33:2 – Thick Slurry

White Oil:Clay:Ethanol – 65:32:3 – Very thick slurry

From the above experiment, it showed an improvement in the second mixture becoming thixotropic. Therefore, further experiments were carried out keeping the clay to ethanol concentration ratio constant at 9%.

From the literature, it was reported that 1-5% of clay should be used in order to achieve the desired properties and above that level, the properties are deteriorating (Ma et al., 2012). However, it is important that clay should disperse in white oil at lower levels without showing any phase separation. Therefore, seven samples were prepared as shown in Table 2.

Table 2: Formulations with White Oil, Clay and Ethanol

Component/Formula	1	2	3	4	5	6	7
Clay (wt.%)	16.42	21.45	27.85	29.81	31.73	33.22	34.74
White Oil (wt.%)	82.10	76.62	69.64	67.57	65.42	63.85	62.12
Ethanol (wt.%) (9% of Clay)	1.48	1.93	2.51	2.62	2.86	2.93	3.14

From the above experiment, it was observed that as the amount of clay increased, less oil was observed at the surface and single phase mixture was only observed after passing levels above 11 g (almost 30% of the total formulation) of clay.

It is clear that ethanol cannot be used as activator in order to improve the compatibility between the clay and the white oil since high concentration of clay is required. Therefore, at this point, something else is needed in order to allow the reduction of the clay content of the matrix.

Activator with a -COOH functional group

Another polar group chosen was carboxylic group (-COOH) in two different carbon chain length acids namely acetic acid and stearic acid. Firstly three formulations were prepared with acetic acid replacing ethanol as follows:

Table 3: Formulations with White Oil, Clay and Acetic acid

Component/Formula	1	2	3
Clay (wt.%)	16.42	27.86	33.19
White Oil (wt.%)	82.10	69.64	63.82
Acetic acid (wt.%) (9% of Clay)	1.48	2.51	2.99

It was observed that at 16.4 wt.% of clay concentration, there was a phase separation of white oil from the clay. At 27.9 wt.%, it seemed like the white oil was completely absorbed by clay showing single phase mixture and it was thixotropic. At 33.2 wt.% of clay concentration, the mixture was like thick putty.

Again, higher clay contents were required in order for the white oil to be completely absorbed by clay without showing any phase separation.

Finally, stearic acid was used in an attempt to achieve a single phase mixture of white oil and clay at very low levels of clay having a workable viscosity. To do this, the carboxylic group concentration was calculated in 9 % acetic acid. The concentration of stearic acid was adjusted to represent the same carboxylic acid content in the formulation. Two formulations were prepared in which only the concentration of clay was different which are as follows:

Table 4: Formulations with White Oil, Clay and Stearic acid

Component/Formula	1	2
Clay (wt.%)	16.16	27.82
White Oil (wt.%)	69.95	60.22
Stearic Acid (wt.%)	13.90	11.96

It was observed that at 16.2 wt.% of clay concentration, the mixture was thixotropic without any phase separation whereas at 27.8 wt.% of clay concentration, it was like thick putty. It is more likely to show the same results at even lower levels of clay. Therefore, citronellal (repellent) was added in the next formulation and clay concentration was reduced to 5 % keeping the stearic acid concentration the same to achieve a single phase mixture with workable viscosity which is as follows:

Table 5: Formulations with White Oil, Clay, Stearic acid and Citronellal

Component	Mass (g)	Proportion (wt.%)
Clay	2.52	5.0
White oil	31.98	64.0
Stearic acid	2.02	4.0
Citronellal	13.47	27.0

In order to achieve the correct citronellal concentration in the above formulation, a quick experiment was done by adding citronellal into clay and EVA polymer separately to see how much it is being absorbed by the two. From the above formulation in Table 5, a single phase mixture was obtained having good flow properties.

Comparison of formulations with EVA and LLDPE

Once the desired formulation was achieved, it was the time to replace the white oil with either EVA or LLDPE. Therefore, two formulations (Table 6) were

prepared on a twin screw micro extruder (Figure 18). The aim of this exercise was to determine which formulation absorbs the most citronellal if they are left immersed in it for few days.

Figure 18: Thermo Scientific Micro Twin Screw Extruder, Sample size = 5g

Table 6: Formulations with EVA, LLDPE, Clay and Stearic acid

Component	Formula 1* Proportion (wt.%)	Formula 2* Proportion (wt.%)
EVA	91.0	-
LLDPE	-	91.0
Clay	5.0	5.0
Stearic Acid	4.0	4.0

*Conditions at which the samples were prepared are as follows:

Formula 1: Temperature 130 C, Screw Speed: 50 rpm, mixing time: 30 min

Formula 2: Temperature 140 °C, Screw Speed: 50 rpm, mixing time: 30 min

Table 7: Immersion test results of Table 6 formulations

	Formula 1	Formula 2
Initial weight (g)	0.156	0.058
Final weight after 4 days (g)	0.195	0.062
Absorption of citronellal (%)	25.0	6.9

From Table 7, it was concluded that EVA copolymer would be the right candidate to design a product which can retain more citronellal and then slowly release it over an extended period of time. This phenomenon can also be explained due to higher amorphous regions in EVA copolymer compared to LLPDE. The choice of EVA copolymer can be crucial since it is commercially available in different VA contents with different MFIs and which can greatly affect the final properties of the polymer nanocomposites (Joseph and Focke, 2011, Marini et al., 2009, Shi et al., 2009, Zhang et al., 2003). It also depends on the processing technique to be used (Gupta et al., 2005, Sridhar et al., 2012).

Proposed formulations for characterization

Following formulations were prepared using a twin screw micro extruder.

Table 8: Proposed formulations for characterization

Formulation	Component (wt.%)			
	EVA (E)	Clay (C)	Stearic acid (S)	Citronellal (Ci)
E/C5	95	5	-	-
E/C5/S	91	5	4	-
E/C5/S/Ci	66	5	4	25
E/C2.5/S/Ci	68.5	2.5	4	25
E/C7/S/Ci	64	7	4	25
E/Ci	75	-	-	25

Mass loss Test

Six formulations were prepared using industrial twin screw extruder, all containing citronellal at 25 % and then left inside the oven at 40, 50 and 60 °C

respectively. Each sample was weighed every day in order to determine the slow release of citronellal.

Table 9: Formulations for Mass loss test

Formulation	Component (wt.%)			
	EVA (E)	Clay (C)	Stearic acid (S)	Citronellal (Ci)
E/S/Ci	71	-	4	25
E/C2.5/Ci	72.5	2.5	-	25
E/C5/S/Ci	66	5	4	25
E/C2.5/S/Ci	68.5	2.5	4	25
E/C7/S/Ci	64	7	4	25
E/Ci	75	-	-	25

Conditions at which the samples were prepared are as follows:

Temperatures: Zone 1 - 90 °C, Zone 2 - 120 °C, Zone 3 - 130 °C, Die - 130 °C

Screw Speed: 74 rpm

3.3   Characterization

3.3.1 Thermal Gravimetric Analysis (TGA)

Thermogravimetric measurements were carried out using Mettler Toledo Star System instrument. Samples of around 15 mg each were heated from 25°C to 900°C at a rate of 10°C/min under air flow (flow rate of 50 ml/min). All the samples were tested with identical conditions.

3.3.2 X-Ray Diffraction (XRD)

X- Ray Diffraction (XRD) was performed to characterize the formation of the nanocomposite. XRD patterns were recorded with a PAN analytical X'pert diffractometer equipped with Ni-filtered CoKα radiation (λ = 0.17903 nm) under 40 kV voltage and a 40 mA current. The scanning rate used was 18 min^{-1}. The samples were investigated over a diffraction angle (range of 0–12) at ambient temperature. The clay was analysed as powder and the composites as disks of 2 mm thickness and 10 mm diameter.

3.3.3 Field Emission Scanning Electron Microscopy (FESEM)

The dispersion of clay particles and their orientation was observed using Zeiss Ultra 55 Field Emission Scanning Electron Microscopy at EHT (Extra high tension) = 2.00 kV. The samples were fractured under liquid nitrogen, cut into small pieces, mounted on sample holders so that the fractured part was facing upwards and then coated with graphite with an electrical discharge. Multiple images from various locations at different magnifications were collected to provide an overall assessment of dispersion.

3.4 Results and Discussions

3.4.1 TGA

Figure 19 (a) demonstrates the thermal stability of EVA nanocomposites compared to straight EVA. The two distinctive peaks are shown by all the samples which are due to the presence of vinyl acetate (VA) content which starts to degrade at 320 °C followed by the degradation of polyethylene at 420 °C. It also shows that the addition of clay in any of the given formulations improved the apparent thermal stability of the polymer by 30 - 35 °C in accordance with previous results (Joseph and Focke, 2011).

Mixing time does not affect the thermal properties of the polymer nanocomposites while processing on micro twin screw extruder, as shown in Figure 19 (b).

EVA nanocomposites with different loadings of clay were tried in order to identify the improvement in the slow release of citronellal. It was observed that a formulation with 2.5 % clay content shows a slight improvement in the slow release of citronellal as shown in Figure 19 (c).
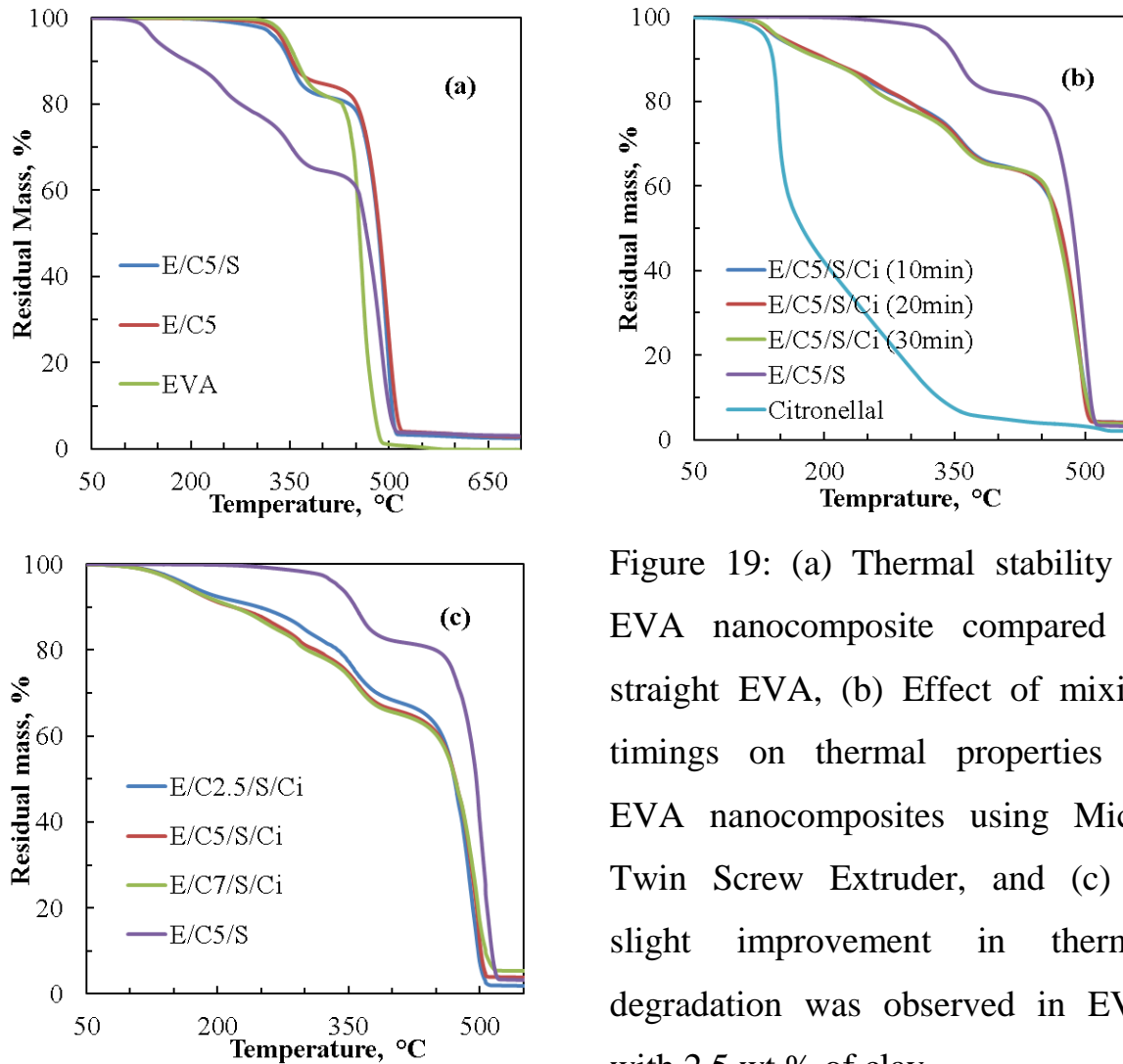
Figure 19: (a) Thermal stability of EVA nanocomposite compared to straight EVA, (b) Effect of mixing timings on thermal properties of EVA nanocomposites using Micro Twin Screw Extruder, and (c) A slight improvement in thermal degradation was observed in EVA with 2.5 wt.% of clay.

3.4.2 XRD

The distance between the clay particles and the mean spacing between clay silicate layers in EVA nanocomposites were obtained using this technique. In Figure 20, it shows the scattering intensity profiles of different formulations of EVA nano-composites. The XRD data of Dellite 43 B clay is also shown in the figure as reference. XRD of the EVA/Clay5/Stearic acid, EVA/Clay5/Stearic acid/citronellal and EVA/Clay7/Stearic Acid/ Citronellal formulations indicate the intercalation of EVA macromolecules into the MMT gallery space, by showing the shift to lower angles from the original clay basal reflection at around $2\theta = 5°$. It also shows that true exfoliation did not take place. The clay

layers remained in a stacked, but expanded form inside the polymer. As expected the intensity of the reflections became more pronounced as the clay loading increased. Furthermore the d-spacing is unaffected by the clay concentration as shown in Table 10.
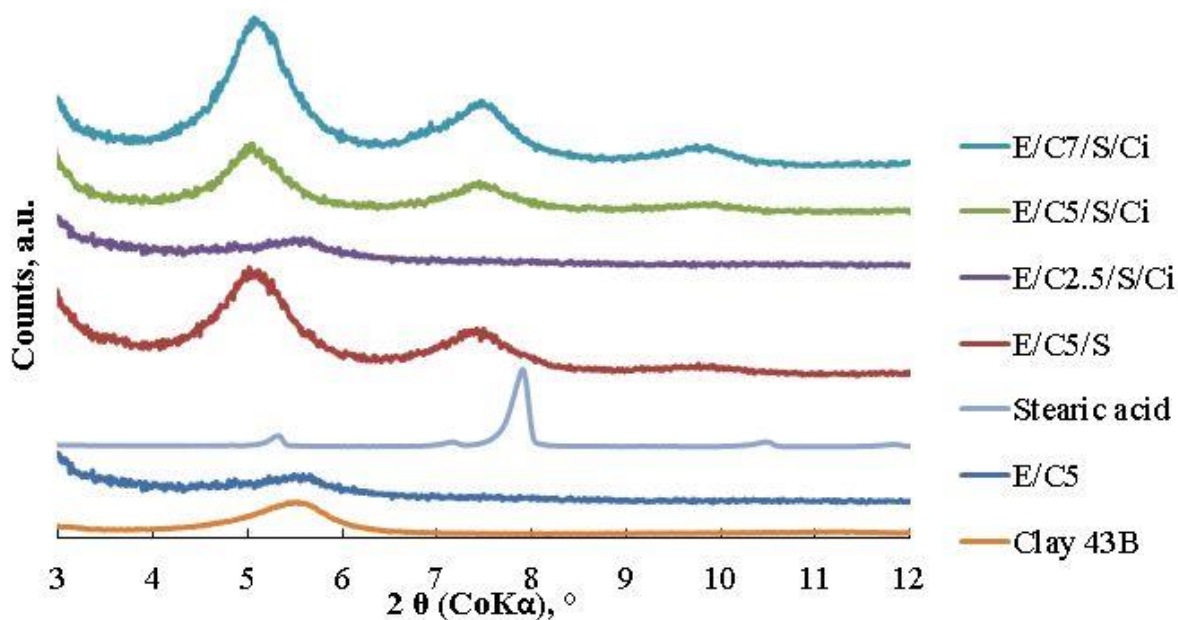
Figure 20: XRD peaks of different formulations showing the shift to lower angles from the original clay basal reflection at around $2\theta = 5°$. E = EVA, C = clay, number = amount of clay added in wt.%, S = stearic acid, Ci = citronellal.

Table 10: XRD results

Sample	Diffraction angle (°)	d-spacing (nm)	d- change (%)
Dellite 43B	5.501	1.865	0
E/C5	5.618	1.826	-2.09
E/C5/S	4.965	2.067	10.83
E/C2.5/S/Ci	5.002	2.051	9.97
E/C5/S/Ci	5.004	2.051	9.97
E/C7/S/Ci	5.109	2.008	7.67

3.4.3 FESEM (Morphology)

Figure 21 suggests that the clay particles are orientated in one direction. Figure 21 (a) seems to show a finer dispersion than is seen the other formulations. It suggests that a formulation without stearic acid could work better in terms of slowing the release rate of citronellal due to the higher aspect ratio of the clay.
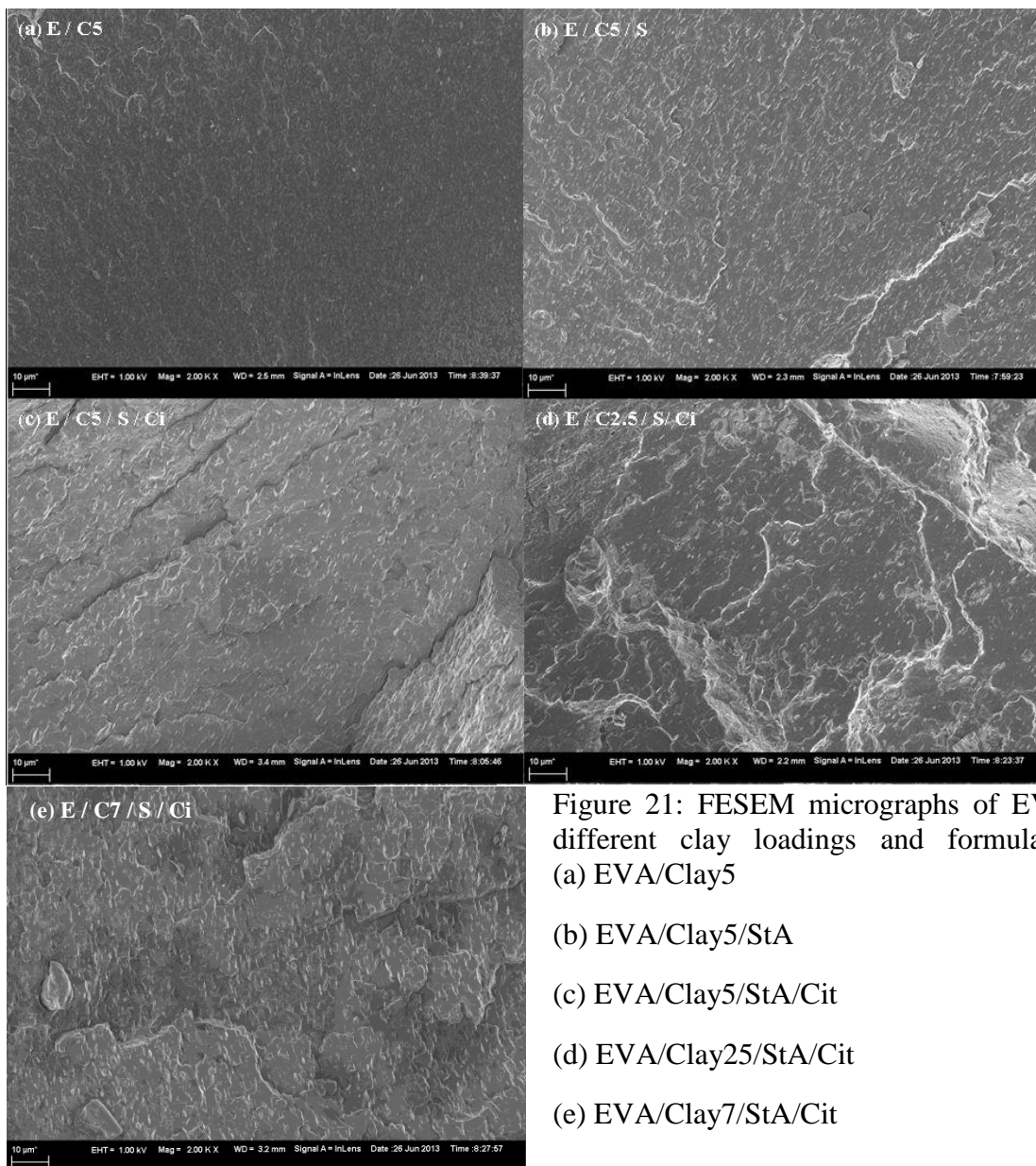
Figure 21: FESEM micrographs of EVA at different clay loadings and formulations, (a) EVA/Clay5

(b) EVA/Clay5/StA

(c) EVA/Clay5/StA/Cit

(d) EVA/Clay25/StA/Cit

(e) EVA/Clay7/StA/Cit

3.4.4 Mass loss

From Figure 22 (a), (b) and (c), it was found that all the formulations released a significant amount (about 15-20%) of citronellal within one day except for the

formulation without stearic acid (E/C2.5/Ci). This difference can be attributed to the loss of citronellal during processing which is clearly indicated by the plateauing of its curve.
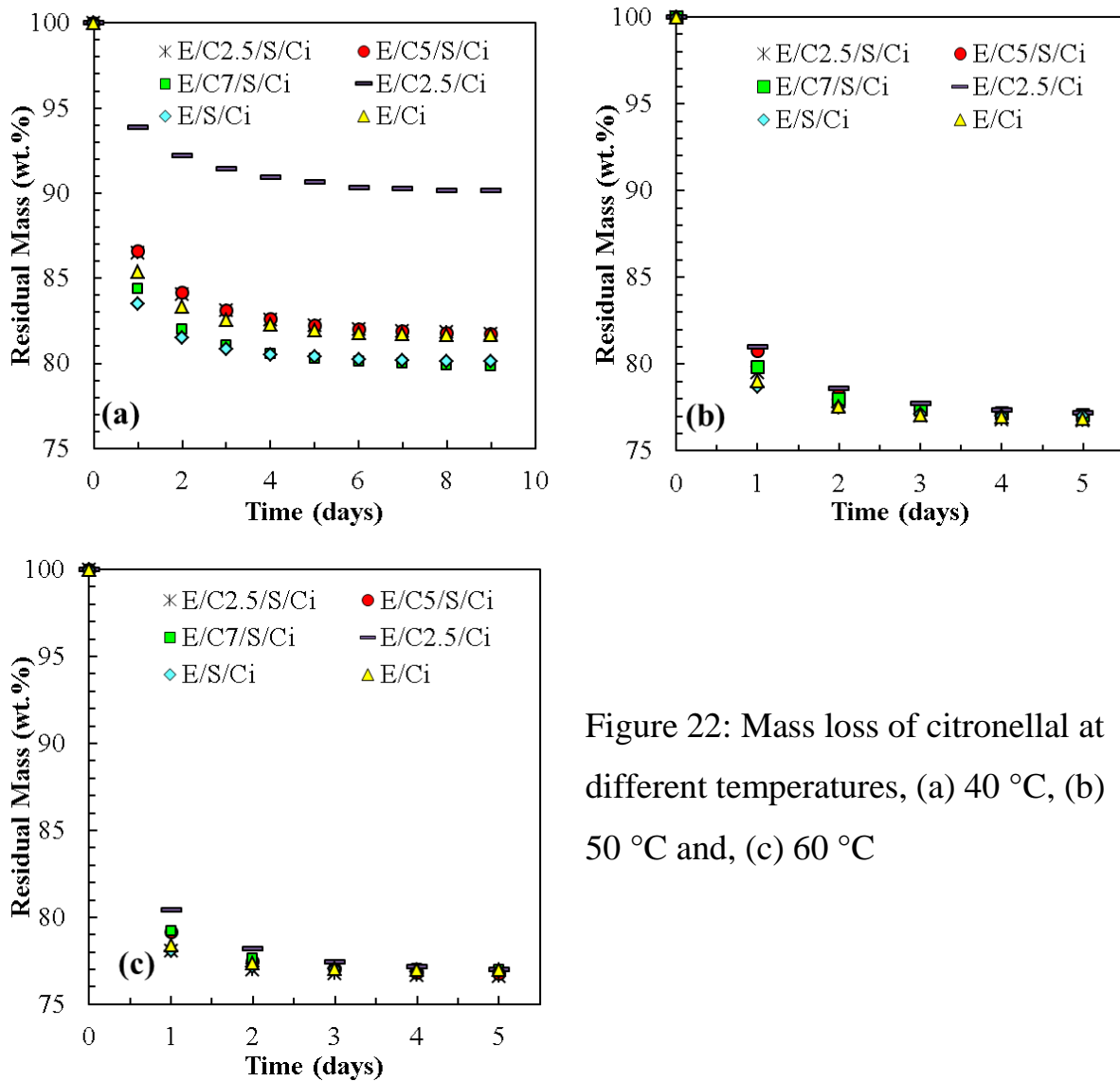
Figure 22: Mass loss of citronellal at different temperatures, (a) 40 °C, (b) 50 °C and, (c) 60 °C

4   Second Concept

4.1   Introduction

On the basis of the above study, another idea was developed in which a polymer was used that does not interact strongly with the repellent. This means that the repellent will not be soluble in such a polymer matrices at the end-use temperature. So another way to trap the repellent must be found. Usually solubility is enhanced at elevated temperatures. At sufficiently high temperatures, corresponding to typical polymer processing temperature, many polar compounds form homogeneous solutions even with highly nonpolar polymers such as polyethylene. Rapid cooling of such mixtures to sub-zero temperatures leads to the formation of co-continuous phase structures. In essence the polymer phase becomes open cell microporous structure with the repellent trapped inside (Castro, 1981). Figure 23 shows a scanning electron micrograph of such a structure.
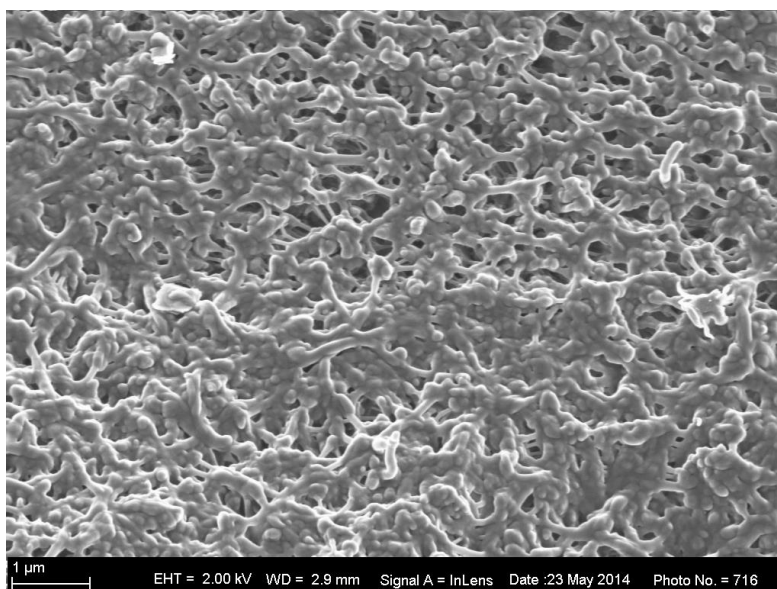
Figure 23: Example of a co-continuous phase structure

Better control of the repellent release rate will be possible with a membrane-like structure. When diffusion of the active through the membrane is the mass

transport limiting step, a more gradual reduction in the release rate over time is realized. The permeability of membranes with respect to a particular active ingredient can be engineered by adjusting the membrane thickness and judicious selection of the polymer system to be used as matrix.

In this work, linear low density polyethylene (LLDPE) with 3,7-dimethyloct-6-en-1-al (citronellal) was used to form the microporous structure via the TIPS process. The focus of this study was to understand the phase behaviour of its mixture using Flory-Huggins (F-H) model and the morphology of the microporous structures formed at different quenching depths.

4.2   Experimental

4.2.1   Materials

Linear low density polyethylene (LLDPE) (Grade HR 411: MFI 3.5 @190°C, 2.16 kg); density 0.939 g/cm^3; particle size: 90% < 600 μm) was supplied by Sasol Polymers. According to the manufacturer, the M_n, M_w, M_z, and polydispersity values for this material were respectively 50447 gmol^{-1}, 170155 gmol^{-1}, 512752 gmol^{-1}, and 3.37.

Citronellal (3,7-dimethyloct-6-en-1-al), ethanol (97%) and ethylene glycol were obtained from Merck Chemicals.

4.2.2   Methods

Sample preparation for quenching temperatures: Samples containing LLDPE/citronellal were prepared at the ratio of 40:60 on an industrial aluminium foil and then folded in such a manner as to prevent diluent from escaping upon heating. The samples were then placed in an oven at 150 °C for an hour and a half to homogenize the solution, and were then quenched cooled by immersing in containers having different mixtures of ethanol and ethylene

glycol with dry ice (Lee and Jensen, 2000) to give different quenching temperatures of -18°C, -14°C and 5°C. One sample of each was also quenched cooled in liquid nitrogen at around -171°C.

4.3 Characterization

4.3.1 Differential scanning calorimetry (DSC)

Perkin Elmer DSC4000 equipment (Figure 24) was used to determine the dynamic crystallization onset temperature (T_c) under N_2 atmosphere to minimize thermal degradation. The samples were sealed at different LLDPE/Citronellal ratios of 10:90, 20:80, 30:70, 40:60 and 50:50 in aluminium pans and the experiments were executed according to the following program: (1) Initial temperature of 30°C, (2) heated to 145°C at a heating rate of 40°C min^{-1}, (3) held at 145°C for 5 min, (4) cooled to 30°C at a cooling rate of 40°C min^{-1}, (5) Held at 30°C for 5 min. Repeated step 2-5 twice for homogenous solution then (6) heated to 145°C at a heating rate of 40°C min^{-1}, (7) held at 145°C for 5 min, (8) cooled to 30°C at a cooling rate of 10°C min^{-1}, (9) Held at 30°C for 2 min.
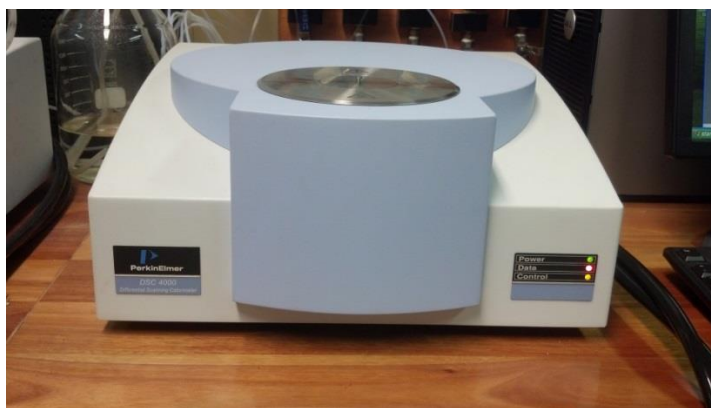
Figure 24: Perkin Elmer DSC 4000

4.3.2 Hot stage optical microscopy (OM)

A Leica DM2500M optical microscope was used to determine the Cloud point temperature (T_{cloud}) which was equipped with Leica DFC420 video camera to take pictures and Linkam CSS 450 hot stage for melting the sample as shown in

Figure 25. Leica Materials Workstation (Version V 3.6.1) software was used to analyse samples visually and Linksys32 (Version 1.9.5) software for setting up temperature profile connected to hot stage. Samples of LLDPE/Citronellal were weighed on glass disc according to the ratios mentioned above and then each sample was placed sequentially between the two top and bottom plates of the hot stage. The experiment was set on to Linksys32 (Version 1.9.5) software according to the following sequence: (1) Heated to 145°C at 30°C min^{-1} (2) Held at 145°C for 5 min (3) Cooled to 100°C at 30°C min^{-1} (4) Held at 100°C for 5 min. Repeated step 1 and 2 for homogenous solution, then (5) Cooled to 30°C at 10°C min^{-1} and determined the cloud point temperature (T_{cloud}) where turbidity would appear visually in the solution.

Figure 25: Leica DM2500M optical microscope equipped with Leica DFC420 video camera

4.3.3 Field Emission Scanning Electron Microscopy (FESEM)

Samples prepared for determining quenching temperatures were then washed with acetone and dried to remove any traces of citronellal. The dried samples were then fracture broken under liquid nitrogen and then electrically discharged coated with graphite. The microporous structure of the samples was observed using Zeiss Ultra 55 Field Emission Scanning Electron Microscopy at EHT (Extra high tension) = 2.00 kV.

4.4 Results

4.4.1 Differential scanning calorimetry

Figure 26 shows representative cooling curves obtained by DSC. It is clear that LLDPE in citronellal showed a clear demixing zone before the crystallization curve, in which liquid-liquid phase separation has taken place. This can be attributed to LLDPE and Citronellal reaching the homogenous solution. It was also observed that the presence of citronellal causes a shift in the position of the crystallization peak position to lower temperatures. Its presence delays the onset of crystallization most likely due to a freezing point depression effect.
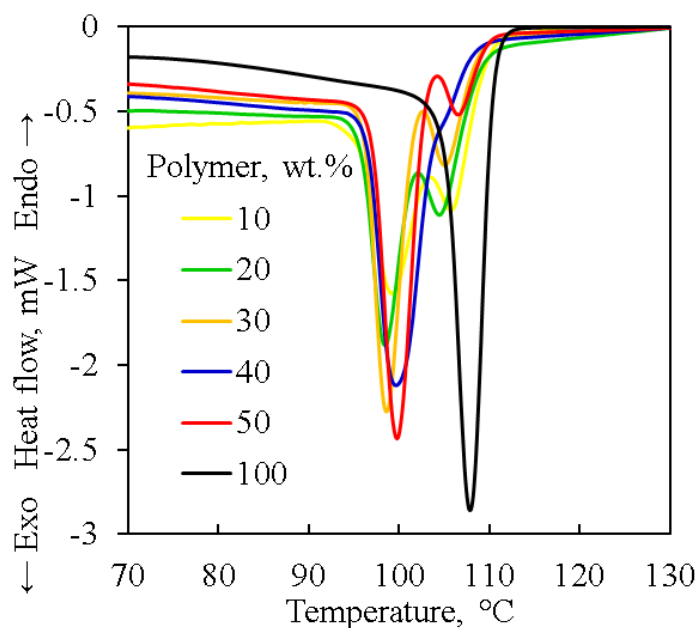
Figure 26: DSC crystallization curves for LLDPE/Citronellal obtained at a scan rate of 10°C min^{-1} clearly showing the demixing exotherm.

The heat of demixing and crystallization was determined from DSC curves obtained at different mixing ratios by calculating the area under the curve as shown in Figure 27. For the heat of crystallization, obtained from cooling curves, an increasing trend was observed with increasing polymer volume fraction as expected. A slight deviation from a straight line indicates that some LLDPE may have dissolved in citronellal and therefore did not crystallize. The heat of demixing showed an apparent minimum at ca. 20 vol.% polymer.
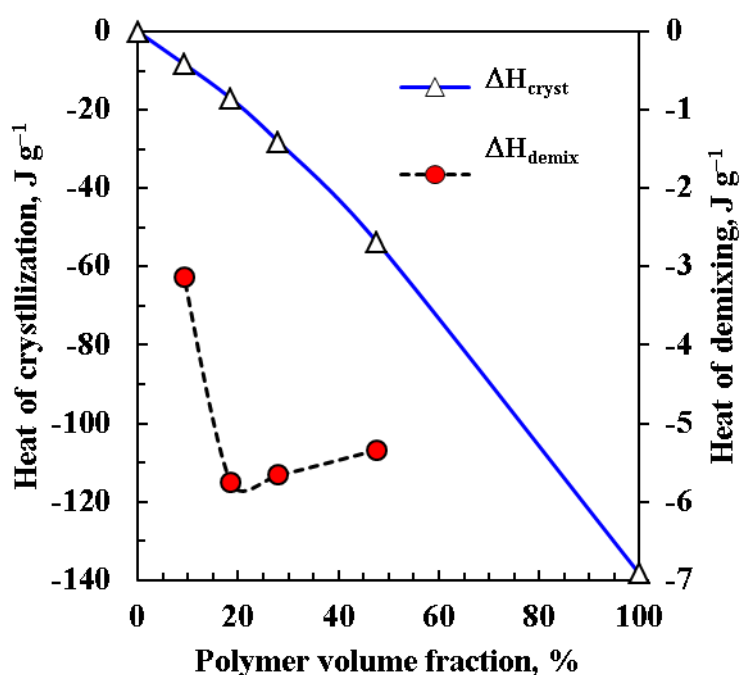
Figure 27: DSC crystallization and demixing enthalpies for LLDPE/Citronellal measured at a scan rate of 10°C min^{-1}.

4.4.2 Hot stage optical microscopy

Optical micrographs of LLDPE/Citronellal mixture were obtained using hot stage optical microscopy in order to determine the cloud points (appearance of turbidity). The samples were taken above the melting temperature of LLDPE at 140°C to ensure the materials are miscible into each other without any apparent boundary lines in the mixture. Subsequently, samples were cooled at a constant

rate of 10°C min^{-1} and as the mixture started to change its texture, that point was taken as the cloud point. Later, crystals appeared in the mixture upon further cooling. Figure 28 shows representative phase changes in the binary system observed under optical microscopy.
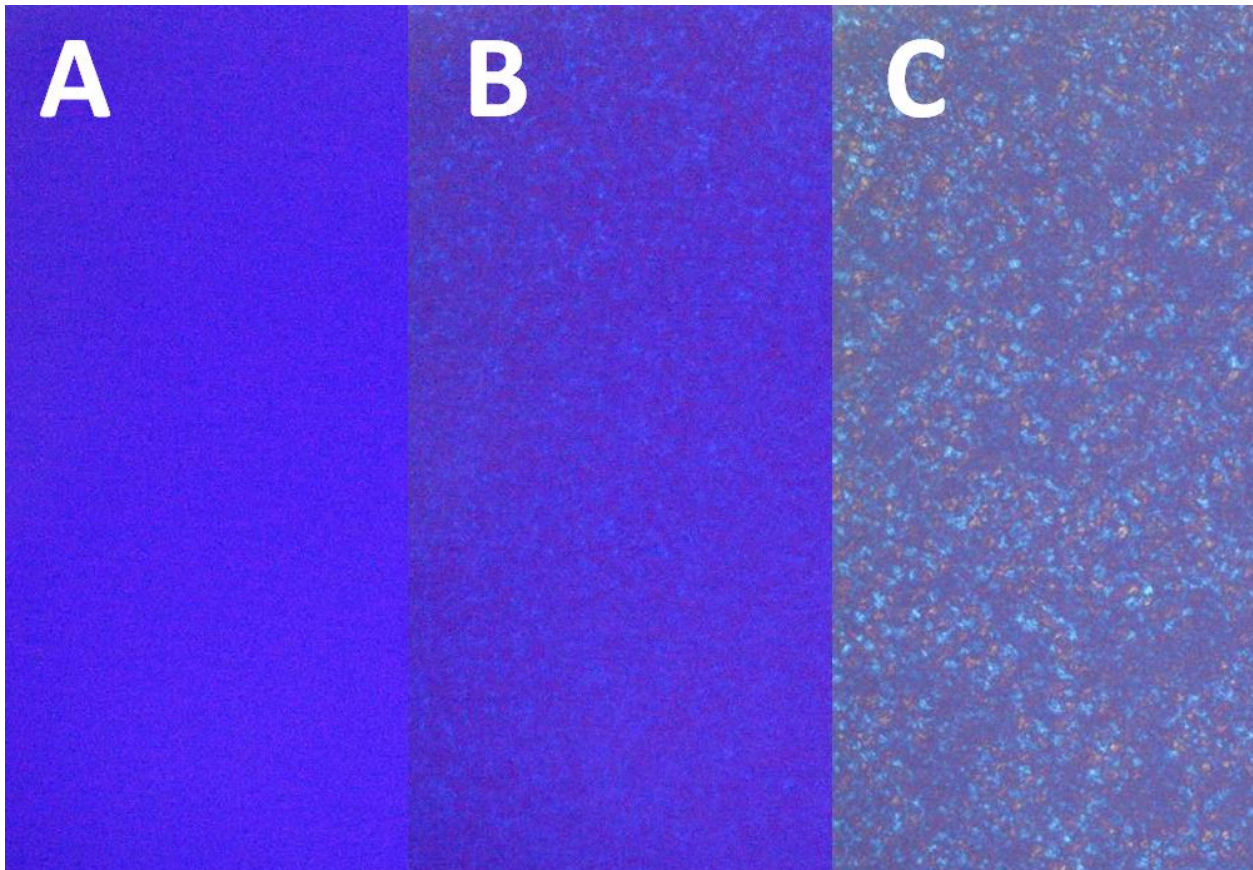
Figure 28: Optical micrographs of phase changes in a binary system containing 30 wt.% LLDPE and 70 wt.% citronellal. (A) Homogeneous mixture at 140°C; (B) appearance of turbidity at 108°C, and (C) solidified crystalline material at 80°C.

4.5 Discussion:

4.5.1 Phase diagram

According to Flory-Huggins (F-H) theory, the Gibb's free energy of mixing per lattice site can be expressed as (Lovell, 2011):

$$\Delta G_{mix} = \Delta H_{mix} - T\Delta S_{mix} \qquad (12)$$

$$\Delta G_{mix} = RT[n_1 ln\phi_1 + n_2 \ln \phi_2 + n_1 \phi_2 \chi] \qquad (13)$$

where ϕ_1 and ϕ_2 are the volume fractions of solvent and polymer respectively, n_1 and n_2 are the number of mols of solvent and polymer respectively, χ is the F-H interaction parameter, R is the molar gas constant and T is the temperature. Equation (13) was independently derived by Flory and Huggins and is commonly called as F-H equation.

For polymer solutions Equation (13) can be re-written as,

$$\Delta \bar{G}_{mix} = RT \left[(1 - \phi_2) \ln(1 - \phi_2) + \frac{\phi_2}{x} \ln\phi_2 + \chi(1 - \phi_2)\phi_2 \right] \qquad (14)$$

where $\Delta \bar{G}_{mix}$ is the Gibbs free energy of mixing per mole of lattice sites, x is the ratio of the polymer molar volume to the solvent molar volume as shown in Equation (19).

$$x = (M_{n.2}/\rho_2)/(M_1/\rho_1) \qquad (19)$$

where $M_{n.2}$ is the number average molecular weight of polymer, M_1 is the molecular weight of solvent, ρ_1 and ρ_2 are the densities of solvent and polymer respectively.

Binodal curve: McGuire (McGuire et al., 1994) proposed a simple method for extrapolating the co-existence or binodal curve (liquid–liquid phase boundary) from experimental cloud point measurements. He presented two Equations (20) and (21), equating the polymer's chemical potential to elaborate the two separate phases (binodal line):

$$\left[\left(\phi_2^\beta \right)^2 - (\phi_2^\alpha)^2 \right] \chi = \ln \left(\frac{1 - \phi_2^\alpha}{1 - \phi_2^\beta} \right) + \left(1 - \frac{1}{x} \right) \left(\phi_2^\alpha - \phi_2^\beta \right) \qquad (20)$$

$$x \left[\left(1 - \phi_2^\beta \right)^2 - (1 - \phi_2^\alpha)^2 \right] \chi = \ln \left(\frac{\phi_2^\alpha}{\phi_2^\beta} \right) + (x - 1) \left(\phi_2^\alpha - \phi_2^\beta \right) \qquad (21)$$

where, ϕ_2^{α} is the polymer's volume fraction in the polymer-poor phase, and ϕ_2^{β} is the polymer volume fraction in the polymer-rich phase.

As a first approximation, the cloud points were assumed to be representative of the coexistence curve. Converting the experimental cloud point measurements from weight percentage to volume fraction and then using these as ϕ_2^{β} and simultaneously solving Equation (20) and (21), the interaction parameters χ was calculated.

It was also assumed that χ is only dependent on temperature and can be expressed as

$$\chi = a + (b/T) \tag{11}$$

where term 'a' is referred to as 'entropic part' of χ and term 'b/T' is referred to as 'enthalpic part'.

Using Equation (11), interaction parameter, χ, versus $1/T$ was plotted in Figure **29**. A linear relationship was observed across the experimental composition range which describes the binary system to have UCST (Rubinstein and Colby, 2003).
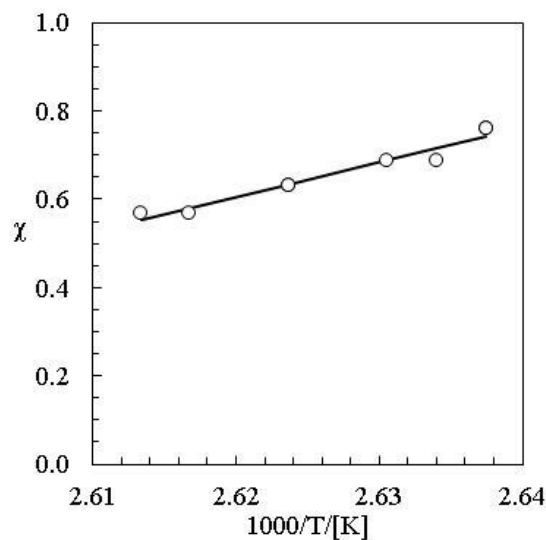
Figure 29: Temperature dependence of interaction parameter

Spinodal curve: Spinodal compositions can be determined by the application of the condition $(\partial^2 \Delta G_{mix}/\partial \phi_2^2)^{\alpha,\beta} = 0$ on Equation (14) giving the following expressions (Lovell, 2011):

$$\frac{1}{(1-\phi_2^\alpha)} + \frac{1}{x\phi_2^\alpha} - 2\chi = 0 \tag{22}$$

$$\phi_2^\beta = 1 - \frac{1}{\sqrt{2\chi}} \tag{23}$$

Critical point: Since the binodal and spinodal curves coincides at the turning point which is the critical temperature (T_{crit}), therefore the critical composition ($\phi_{2(crit)}$) can be determined by the application of the condition $(\partial^3 \Delta G_{mix}/\partial \phi_2^3) = 0$ to give the following expression (Lovell, 2011),

$$\phi_{2(crit)} = \frac{1}{1 + \sqrt{x}} \tag{24}$$

By substituting Equation (24) into (22), critical value (χ_{crit}) of the F-H interaction parameter is obtained.

$$\chi_{crit} = \frac{1}{2}\left(1 + \frac{2}{\sqrt{x}} + \frac{1}{x}\right) \tag{25}$$

This in turns would give the critical temperature (T_{crit}) by simply substituting the value of χ_{crit} into Equation (11) as

$$T_{crit} = \frac{b}{\chi_{crit} - a} \tag{26}$$

Using all the above expressions, the coexistence curves (binodal and spinodal) were plotted in Figure 30 along with the cloud points. The generation of the coexistence curves in this manner is essentially an elegant curve fit based on Flory's theory.

4.5.2 Determination of melting and crystallization point depression curve

The melting and crystallization point depression curve were also predicted in Figure 30 along with the experimental melting and crystallization temperatures using the following expression (McGuire et al., 1994),

$$
\frac{1}{T_{m,c}} = [1 + \frac{Rb}{\Delta H_u}(1 - \phi_2)^2]^{-1}\left\{\frac{1}{T_{m,c}^{\circ}}\right.
$$
$$
\left. + \frac{R}{\Delta H_u}\left[\left(1 - \frac{1}{x}\right)(1 - \phi_2) - \frac{ln\phi_2}{x} - a(1 - \phi_2)^2\right]\right\}
$$

(27)

where $T_{m,c}$ is the maximum melting temperature or crystallization onset temperature of the diluted polymer depending on the set of data under observation. Similarly, $T_{m,c}^{\circ}$ is the maximum melting temperature or crystallization onset temperature of the pure polymer and ΔH_u is the heat of fusion or crystallization per mole of volume segments (see Appendix 1 for unit conversion of ΔH_u).
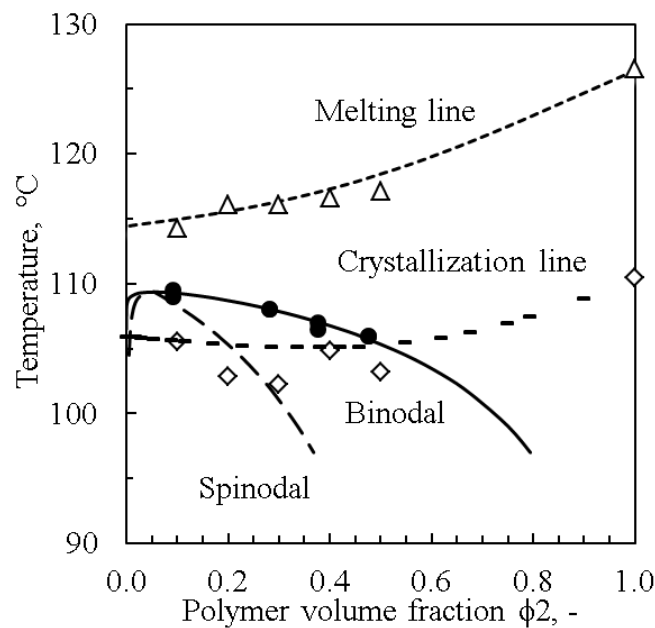
Figure 30: Experimental and predicted phase diagrams of LLDPE in Citronellal

Figure 30 shows the phase diagram of LLDPE and citronellal blends having UCST type phase behaviour. For the predicted binodal and spinodal curve, it was assumed that the experimental cloud points are the representative of the binodal curve which turns out to be a good match of Flory-Huggins model. Experimental melting points of the mixtures also coincided well with the predicted melt depression curve as well as the experimental crystallization onset points with the predicted crystallization depression curve which determines the quenching depth of the system.

The phase diagram shows that at temperatures higher than the melting temperature of LLDPE, all the mixtures exhibited a homogenous solution, upon heating. Upon cooling of the mixtures, as soon as the temperature hit the crystallization depression curve, LLDPE started crystallizing and solid – liquid phase separation occurred.

From the predicted binodal curve, it shows that at lower temperatures below the binodal curve, LLDPE is poorly soluble in citronellal. It also shows from the predicted spinodal curve that the concentration of LLDPE can be 50% or lower in order to hit the spinodal region well below 90 °C to attain the co-continuous structure morphology. This can only be achieved if the predicted crystallization depression curve can be shifted down at lower quenching depths by means of quench cooling the system at higher rates (Li, 2006).

4.5.3 Determination of quench depth and morphology

Different quenching temperatures were applied to LLDPE/citronellal mixtures at 40:60 ratios in order to determine the appropriate quench cooling temperature or quenching depth. It was observed that for LLDPE/citronellal mixture, at all the quenching temperatures, it gave the same morphology and showed co-continues phase (spinodal decomposition mechanism) as shown in Figure 31.

This behaviour was expected from the DSC results as well as the phase diagram obtained using Flory-Huggins model.

The FESEM results also showed that LLDPE/citronellal mixture can be prepared at quenching temperature of 5 °C as shown in Figure 31(d), which in turn excludes the use of dry ice, ethanol and ethylene glycol mixture (Lee and Jensen, 2000). A simple ice bath can be therefor be used to quench cool and to prepare microporous LLDPE structure with citronellal.
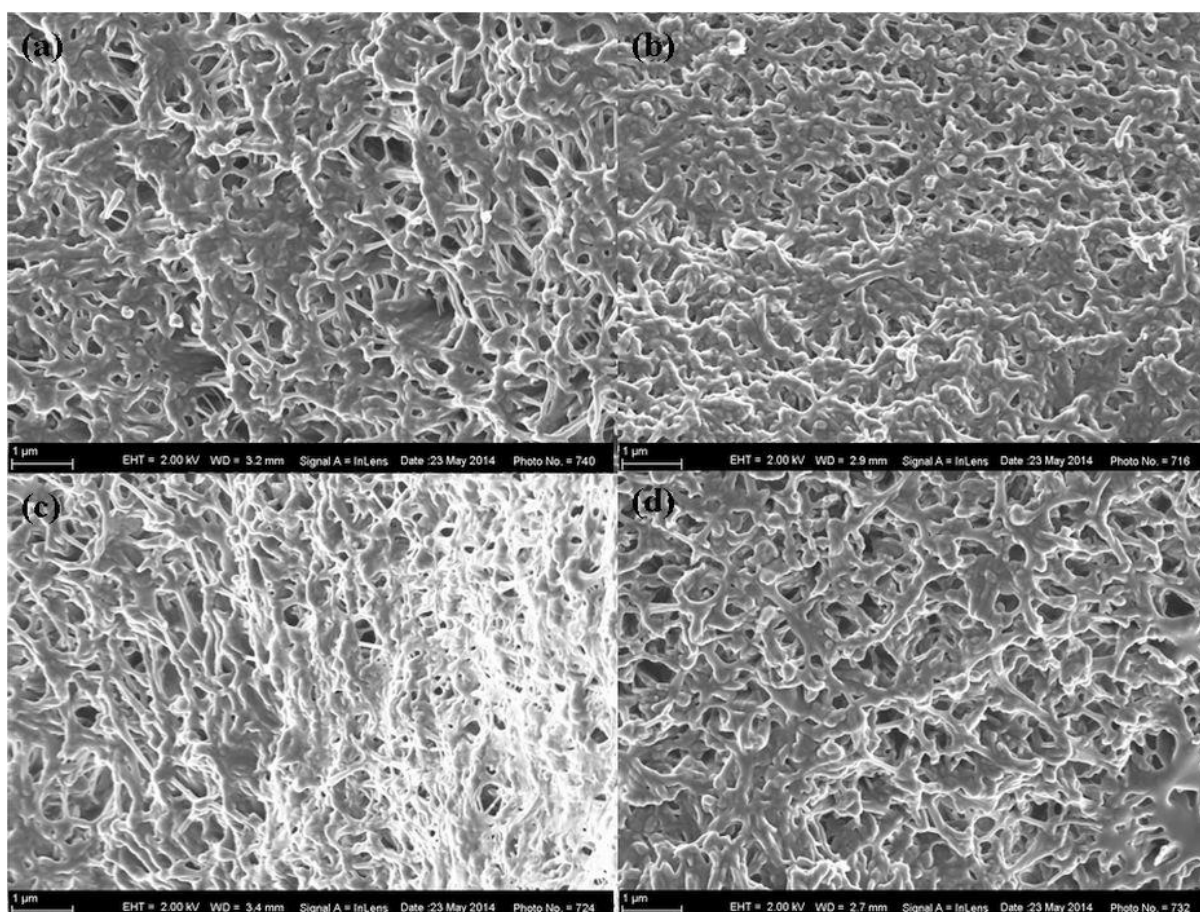
Figure 31: Scanning electron micrographs of LLDPE/Citronellal, 40:60, at different quenching temperatures(a)-171 °C (Liquid Nitrogen) (b)-18 °C (c) -14 °C (d) 5 °C

5   Conclusions and recommendations

The purpose of this study was to investigate ways to control the release rate of highly volatile natural mosquito repellents from polymer matrices, e.g. repellent bracelets and anklets. The ultimate goal is to develop products which can be used for longer periods of time, e.g 2-3 months. Towards this goal, preliminary experiments were performed using citronellal. It is the main constituent of the natural repellent citronella oil. Two approaches were considered for incorporating it in the polymer matrix.

In the first study, citronellal was dissolved in an EVA matrix and the release was hindered by the presence of clay nanoplatelets. The impermeable clay sheets were expected to decrease the release rate by creating a tortuous diffusion path. Initial experiments led to the belief that adding stearic acid would assist the intercalation/exfoliation and dispersion of the clay in the EVA polymer matrix. Further investigation showed that this was not the case. It was also found that, even though plain EVA/clay nanocomposites featured a good dispersion of the clay, it failed to retard the release of citronellal from the EVA nanocomposite. This observation could be attributed to poor interaction between the polymer and citronellal and further investigation is required with respect to the choice of the polymer and/or clay. Another explanation could be the more-or-less random orientations of the clay platelets in the matrix. Barrier properties can be improved when the clay particles are oriented perpendicularly to the diffusion direction.

More importantly, it was found that no more than 20 wt.% citronellal could be incorporated into the EVA. Above this level, the repellent tended to exude leaving oiliness on the polymer surface. In order to generate long-life ankle bracelets, the polymer matrix must be able to both hold large quantities of the

repellent in addition to releasing them slowly at an effective rate. The first issue was deemed more important to investigate. This is justified by the realisation that it would be more appropriate to use a membrane-like barrier to control the rate of release. Hence, the project was modified and the objective revised to focus on ways to increase the amount of repellent that can be incorporated into the polymer so that it can act as a reservoir.

A membrane coating could provide a near constant rate of release of the volatile repellent. It might take the form of a polymer nanocomposite with the dispersed flakes reducing the permeability. However, the design and testing of the membrane concept fell outside the scope of the present investigation.

The idea that was explored presently was to develop a microporous polymer matrix with citronellal as a solvent via thermally induced phase separation method. Clearly the polymer should be insoluble in repellent to facilitate the release. This was achieved using LLDPE as a host polymer to trap citronellal in the matrix. The phase behaviour of this system was modelled with the Flory-Huggins lattice theory. Initial DSC investigations showed that demixing occurred before crystallization of the polymer commenced. This also indicated that heating the mixture to high enough temperatures should give a homogenous solution. Next, clouds points were measured using hot stage optical microscopy. These were used to calculate Flory-Huggins model parameters and predict the extension of the binodal curve (phase envelope). The curve fit of the experimental cloud points (binodal curve) was acceptable. The Flory-Huggins model was then used to predict the location of spinodal curves. It showed that a homogenous mixture of 40 wt. % of LLDPE meets the spinodal curve at 96 °C. A few samples of LLDPE-citronellal (40:60 mass ratios) were quenched cooled to various temperatures. FESEM results showed that at all quenching temperatures, an opened cell microporous structure was obtained, even at 5 °C.

It is recommended to proceed with the above study and find ways to cover the acquired microporous structure with a suitable membrane. This could provide a suitable slow release citronellal dosage form.

6   References

2011. World Malaria Report 2011.

2013. World Malaria Report 2013. *In:* ORGANIZATION, W. H. (ed.).

ABEDIN, F., YE, Q., GOOD, H. J., PARTHASARATHY, R. & SPENCER, P. 2014. Polymerization- and solvent-induced phase separation in hydrophilic-rich dentin adhesive mimic. *Acta Biomaterialia,* 10**,** 3038-3047.

BEEK, W. J., MUTTZALL, K.M.K., VAN HEUVEN, J.W. 1999. *Transport phenomena*, Chichester : Wiley.

BERGAYA, F., THENG, B. K. G. & LAGALY, G. 2006. *Handbook of clay science*, Amsterdam ; London : Elsevier.

BEYER, G. 2002. Nanocomposites: A new class of flame retardants for polymers. *Plastics, Additives and Compounding,* 4**,** 22-28.

BHARADWAJ, R. K. 2001. Modeling the barrier properties of polymer-layered silicate nanocomposites. *Macromolecules,* 34**,** 9189-9192.

BHARADWAJ, R. K., MEHRABI, A. R., HAMILTON, C., TRUJILLO, C., MURGA, M., FAN, R., CHAVIRA, A. & THOMPSON, A. K. 2002. Structure-property relationships in cross-linked polyester-clay nanocomposites. *Polymer,* 43**,** 3699-3705.

CALVERT, P. 1996. When a thick film is thin. *Nature,* 384**,** 311-312.

CANEBA, G. T. & SOONG, D. S. 1985. Polymer membrane formation through the thermal-inversion process. 1. Experimental study of membrane structure formation. *Macromolecules,* 18**,** 2538-2545.

CASTRO, A. J. 1981. Methods for making microporous products.

CHARARA, Z., WILLIAMS, J., SCHMIDT, R. & MARSHALL, M. 1992. Orange flavor absorption into various polymeric packaging materials. *Journal of food science,* 57**,** 963-968.

CHOUDALAKIS, G. & GOTSIS, A. D. 2009. Permeability of polymer/clay nanocomposites: A review. *European Polymer Journal,* 45**,** 967-984.

COCKCROFT, A., COSGROVE, J. & WOOD, R. 1998. Comparative repellency of commercial formulations of deet, permethrin and citronellal against the mosquito Aedes aegypti, using a collagen membrane technique compared with human arm tests. *Medical and veterinary entomology,* 12**,** 289-294.

CUI, Z. Y., XU, Y. Y., ZHU, L. P., WANG, J. Y., XI, Z. Y. & ZHU, B. K. 2008. Preparation of PVDF/PEO-PPO-PEO blend microporous membranes for lithium ion batteries via thermally induced phase separation process. *Journal of Membrane Science,* 325**,** 957-963.

DE GENNES, P. G. 1974. *The physics of liquid crystals*, Oxford : Clarendon.

DE LIMA, J. A. & FELISBERTI, M. I. 2009. Porous polymer structures obtained via the TIPS process from EVOH/PMMA/DMF solutions. *Journal of Membrane Science,* 344**,** 237-243.

FLORY, P. J. 1941. Thermodynamics of high polymer solutions. *The Journal of Chemical Physics,* 9**,** 660-660.

FUNK, C. V. & LLOYD, D. R. 2008. Zeolite-filled microporous mixed matrix (ZeoTIPS) membranes: Prediction of gas separation performance. *Journal of Membrane Science,* 313**,** 224-231.

GERSAPPE, D. 2002. Molecular mechanisms of failure in polymer nanocomposites. *Physical Review Letters,* 89**,** 058301/1-058301/4.

GIANNELIS, E. P. 1996. Polymer layered silicate nanocomposites. *Advanced Materials,* 8**,** 29-35.

GRIMSHAW, R. W. 1980. *The Chemistry and Physics of Clays*, J. Wiley & Sons, New York

GUPTA, R. K., PASANOVIC-ZUJO, V. & BHATTACHARYA, S. N. 2005. Shear and extensional rheology of EVA/layered silicate-nanocomposites. *Journal of Non-Newtonian Fluid Mechanics,* 128**,** 116-125.

HANSEN, C. M. 2000. Hansen Solubility Parameters: A User's Handbook. *CRC Press, Inc.***,** 208

HE, H., MA, Y., ZHU, J., YUAN, P. & QING, Y. 2010. Organoclays prepared from montmorillonites with different cation exchange capacity and surfactant configuration. *Applied Clay Science,* 48**,** 67-72.

HE, H., ZHOU, Q., MARTENS, W. N., KLOPROGGE, T. J., YUAN, P., XI, Y., ZHU, J. & FROST, R. L. 2006. Microstructure of HDTMA+- modified montmorillonite and its influence on sorption characteristics. *Clays and Clay Minerals,* 54**,** 689-696.

HEINZ, H., VAIA, R. A., KRISHNAMOORTI, R. & FARMER, B. L. 2007. Self-assembly of alkylammonium chains on montmorillonite: Effect of chain length, head group structure, and cation exchange capacity. *Chemistry of Materials,* 19**,** 59-68.

HELLMAN, D. J., GREENBERG, A. R. & KRANTZ, W. B. 2004. A novel process for membrane fabrication: thermally assisted evaporative phase separation (TAEPS). *Journal of Membrane Science,* 230**,** 99-109.

HIATT, W. C., VITZTHUM, G. H., WAGENER, K. B., GERLACH, K. & JOSEFIAK, C. MICROPOROUS MEMBRANES VIA UPPER CRITICAL TEMPERATURE PHASE SEPARATION. *In:* LLOYD DOUGLAS, R., ed. Materials Science of Synthetic Membranes. Based on a Symposium at the 187th Meeting of the American Chemical Society., 1985 Washington, DC, USA St Louis, MO, USA. ACS, 229-244.

HTTP://WWW.IVMPROJECT.NET/. [Accessed 12 August 2013].

HUGGINS, M. L. 1941. Solutions of long chain compounds. *The Journal of Chemical Physics,* 9**,** 440-440.

ISHIGAMI, T., KASUYA, Y., RAJABZADEH, S., OHMUKAI, Y., KAKIHANA, Y. & MATSUYAMA, H. 2014. Effect of solidification rate of polymer solution on the die-swell during hollow fiber spinning by non-solvent induced phase separation. *Journal of Membrane Science,* 472**,** 194-201.

ISHII, R., NAKATSUJI, M. & OOI, K. 2005. Preparation of highly porous silica nanocomposites from clay mineral: a new approach using pillaring method combined with selective leaching. *Microporous and Mesoporous Materials,* 79**,** 111-119.

JANEK, M. & LAGALY, G. 2003. Interaction of a cationic surfactant with bentonite: a colloid chemistry study. *Colloid and Polymer Science,* 281**,** 293-301.

JAYNES, W. F. & BOYD, S. A. 1991. Clay mineral type and organic compound sorption by hexadecyltrimethylammonium-exchanged clays. *Soil Science Society of America Journal,* 55**,** 43-48.

JENNIFER & STEVENSON 2012. Novel Vectors of Malaria Parasites in the Western Highlands of Kenya. *Emerging Infectious Diseases* 18**,** 1547-1549.

JONES, T. 1983a. The properties and uses of clays which swell in organic solvents. *Clay Minerals,* 18**,** 399-401.

JONES, T. R. 1983b. The properties and uses of clays which swell in organic solvents. *Clay Minerals,* 18**,** 399-410.

JORDAN, J., JACOB, K. I., TANNENBAUM, R., SHARAF, M. A. & JASIUK, I. 2005. Experimental trends in polymer nanocomposites - A review. *Materials Science and Engineering A,* 393**,** 1-11.

JOSEPH, S. & FOCKE, W. W. 2011. Poly(ethylene-vinyl co-vinyl acetate)/clay nanocomposites: Mechanical, morphology, and thermal behavior. *Polymer Composites,* 32**,** 252-258.

KE, Y. C. & STROEVE, P. 2005. *Polymer-Layered Silicate and Silica Nanocomposites*.

KILIARIS, P. & PAPASPYRIDES, C. D. 2010. Polymer/layered silicate (clay) nanocomposites: An overview of flame retardancy. *Progress in Polymer Science (Oxford),* 35**,** 902-958.

KIM, J. J., HWANG, J. R., KIM, U. Y. & KIM, S. S. 1995. Operation parameters of melt spinning of polypropylene hollow fiber membranes. *Journal of Membrane Science,* 108**,** 25-36.

KIM, J. K., HU, C., WOO, R. S. C. & SHAM, M. L. 2005a. Moisture barrier characteristics of organoclay-epoxy nanocomposites. *Composites Science and Technology,* 65**,** 805-813.

KIM, J. K., KANG, C. S., LEE, J. K., KIM, Y. R., HAN, H. Y. & YUN, H. K. 2005b. Evaluation of Repellency Effect of Two Natural Aroma Mosquito Repellent Compounds, Citronella and Citronellal*. *Entomological Research,* 35**,** 117-120.

KOO, C. M., KIM, S. O. & CHUNG, I. J. 2003. Study on morphology evolution, orientational behavior, and anisotropic phase formation of highly filled polymer-layered silicate nanocomposites. *Macromolecules,* 36**,** 2748-2757.

L.E., N. 1967. Models for the permeability of filled polymer systems. *Macromolecular Science (Chem)***,** 929-942.

LAGALY, G. 1981. Characterization of clays by organic compounds. *Clay Minerals,* 16**,** 1-21.

LAGALY, G. 2006. Chapter 5 Colloid Clay Science. *In:* FAÏZA BERGAYA, B. K. G. T. & GERHARD, L. (eds.) *Developments in Clay Science.* Elsevier.

LAI, M. & KIM, J. K. 2005. Effects of epoxy treatment of organoclay on structure, thermo-mechanical and transport properties of poly(ethylene terephthalate-co-ethylene naphthalate)/organoclay nanocomposites. *Polymer,* 46**,** 4722-4734.

LAN, T., KAVIRATNA, P. D. & PINNAVAIA, T. J. 1994. On the nature of polyimide-clay hybrid composites. *Chemistry of Materials,* 6**,** 573-575.

LEBARON, P. C., WANG, Z. & PINNAVAIA, T. J. 1999. Polymer-layered silicate nanocomposites: An overview. *Applied Clay Science,* 15**,** 11-29.

LEE, D. W. & JENSEN, C. M. 2000. Dry-Ice Bath Based on Ethylene Glycol Mixtures. *Journal of Chemical Education,* 77**,** 629.

LEE, S. Y. & KIM, S. J. 2002. Expansion characteristics of organoclay as a precursor to nanocomposites. *Colloids and Surfaces A: Physicochemical and Engineering Aspects,* 211**,** 19-26.

LI, D. K., W B; GREENBERG, A R; SANI, R L 2006. Membrane formation via thermally induced phase separation (TIPS): model development and validation. *Journal of membrane science,* 279**,** 50-60.

LI, W., YUAN, Y. & CABASSO, I. 1995. FORMATION and microstructure of polyethylene microporous mem-branes through thermally induced phase separation. *Chinese Journal of Polymer Science (English Edition),* 13.

LICCIARDELLO, F., MURATORE, G., MERCEA, P., TOSA, V. & NERIN, C. 2013a. Diffusional behaviour of essential oil components in active packaging polypropylene films by multiple headspace solid phase microextraction–gas chromatography. *Packaging Technology and Science,* 26**,** 173-185.

LICCIARDELLO, F., MURATORE, G., SUMA, P., RUSSO, A. & NERÍN, C. 2013b. Effectiveness of a novel insect-repellent food packaging incorporating essential oils against the red flour beetle (Tribolium castaneum). *Innovative Food Science & Emerging Technologies,* 19**,** 173-180.

LICCIARDELLO, F., MURATORE, G., SUMA, P., RUSSO, A. & NERÍN, C. 2013c. Effectiveness of a novel insect-repellent food packaging incorporating essential oils against the red flour beetle (Tribolium castaneum). *Innovative Food Science & Emerging Technologies,* 19**,** 173-180.

LIZIN, S., VAN PASSEL, S., DE SCHEPPER, E., MAES, W., LUTSEN, L., MANCA, J. & VANDERZANDE, D. 2013. Life cycle analyses of

organic photovoltaics: A review. *Energy and Environmental Science,* 6**,** 3136-3149.

LLOYD, D. R., KIM, S. S. & KINZER, K. E. 1991. Microporous membrane formation via thermally-induced phase separation. II. Liquid-liquid phase separation. *Journal of Membrane Science,* 64**,** 1-11.

LLOYD, D. R., KINZER, K. E. & TSENG, H. S. 1990a. Microporous membrane formation via thermally induced phase separation. I. Solid-liquid phase separation. *Third Ravello Symposium on Advanced Membrane Science and Technology,* 52**,** 239-261.

LLOYD, D. R., KINZER, K. E. & TSENG, H. S. 1990b. Microporous membrane formation via thermally induced phase separation. I. Solid-liquid phase separation. *Journal of Membrane Science,* 52**,** 239-261.

LO, H., KADIYALA, S., GUGGINO, S. E. & LEONG, K. W. 1996. Poly(L-lactic acid) foams with cell seeding and controlled-release capacity. *Journal of Biomedical Materials Research,* 30**,** 475-484.

LÓPEZ, P., SÁNCHEZ, C., BATLLE, R. & NERÍN, C. 2007. Development of flexible antimicrobial films using essential oils as active agents. *Journal of Agricultural and Food Chemistry,* 55**,** 8814-8824.

LOVELL, R. J. Y. A. P. A. 2011. Introduction to Polymers. *CRC Press, Inc.***,** 237-245,310-313.

LU, C. & MAI, Y.-W. 2007. Permeability modelling of polymer-layered silicate nanocomposites. *Composites Science and Technology,* 67**,** 2895-2902.

LUO, B., LI, Z., ZHANG, J. & WANG, X. 2008. Formation of anisotropic microporous isotactic polypropylene (iPP) membrane via thermally induced phase separation. *Desalination,* 233**,** 19-31.

MA, J., DUAN, Z., XUE, C. & DENG, F. 2012. Morphology and mechanical properties of EVA/OMMT nanocomposite foams. *Journal of Thermoplastic Composite Materials,* 26**,** 555-569.

MA, J. & ZHU, L. 2007. Removal of phenols from water accompanied with synthesis of organobentonite in one-step process. *Chemosphere,* 68**,** 1883-1888.

MARINI, J., BRANCIFORTI, M. C. & LOTTI, C. 2009. Effect of matrix viscosity on the extent of exfoliation in EVA/organoclay nanocomposites. *Polymers for Advanced Technologies***,** n/a-n/a.

MASSINGA JR, P. H., FOCKE, W. W., DE VAAL, P. L. & ATANASOVA, M. 2010. Alkyl ammonium intercalation of Mozambican bentonite. *Applied Clay Science,* 49**,** 142-148.

MATSUYAMA, H., BERGHMANS, S., BATARSEH, M. T. & LLOYD, D. R. 1998. Effects of thermal history on anisotropic and asymmetric membranes formed by thermally induced phase separation. *Journal of Membrane Science,* 142**,** 27-42.

MATSUYAMA, H., BERGHMANS, S. & LLOYD, D. R. 1999. Formation of anisotropic membranes via thermally induced phase separation. *Polymer,* 40**,** 2289-2301.

MATSUYAMA, H., HAYASHI, K., MAKI, T., TERAMOTO, M. & KUBOTA, N. 2004. Effect of polymer density on polyethylene hollow fiber membrane formation via thermally induced phase separation. *Journal of Applied Polymer Science,* 93**,** 471-474.

MCGUIRE, K. S., LAXMINARAYAN, A. & LLOYD, D. R. 1994. A simple method of extrapolating the coexistence curve and predicting the melting point depression curve from cloud point data for polymer-diluent systems. *Polymer,* 35**,** 4404-4407.

MEHTA, R. H., MADSEN, D. A. & KALIKA, D. S. 1995. Microporous membranes based on poly(ether ether ketone) via thermally-induced phase separation. *Journal of Membrane Science,* 107**,** 93-106.

MESSERSMITH, P. B. & GIANNELIS, E. P. 1994. Synthesis and characterization of layered silicate-epoxy nanocomposites. *Chemistry of Materials,* 6**,** 1719-1725.

MOONEY, D. J., BALDWIN, D. F., SUH, N. P., VACANTI, J. P. & LANGER, R. 1996. Novel approach to fabricate porous sponges of poly(D,L-lactic-co-glycolic acid) without the use of organic solvents. *Biomaterials,* 17**,** 1417-1422.

MURRAY, C. J. L., ROSENFELD, L. C., LIM, S. S., ANDREWS, K. G., FOREMAN, K. J., HARING, D., FULLMAN, N., NAGHAVI, M., LOZANO, R. & LOPEZ, A. D. 2012. Global malaria mortality between 1980 and 2010: a systematic analysis. *The Lancet,* 379**,** 413-431.

NAMOUNTOUGOU, M., DIABATÉ, A., ETANG, J., BASS, C., SAWADOGO, S. P., GNANKINIÉ, O., BALDET, T., MARTIN, T., CHANDRE, F., SIMARD, F. & DABIRÉ, R. K. 2013. First report of the L1014S kdr mutation in wild populations of Anopheles gambiae M and S molecular forms in Burkina Faso (West Africa). *Acta Tropica,* 125**,** 123-127.

NANCY FULLMAN, R. B., STEPHEN S LIM, CAROL MEDLIN AND EMMANUELA GAKIDOU 2013. Nets, spray or both? The effectiveness of insecticide-treated nets and indoor residual spraying in reducing malaria morbidity and child mortality in sub-Saharan Africa. *Malaria Journal*.

NEWMAN, A. C. D. 1986. *Chemistry of clays and clay minerals*, Harlow : Longman [for] Mineralogical Society.

NUNES, S. P. & INOUE, T. 1996. Evidence for spinodal decomposition and nucleation and growth mechanisms during membrane formation. *Journal of Membrane Science,* 111**,** 93-103.

OKAMOTO, M., NAM, P. H., MAITI, P., KOTAKA, T., HASEGAWA, N. & USUKI, A. 2001. A House of Cards Structure in Polypropylene/Clay Nanocomposites under Elongational Flow. *Nano Letters,* 1**,** 295-298.

OLPHEN, H. V. & FRIPIAT, J. J. 1979. *Data handbook for clay materials and other non-metallic materials*, Oxford : Pergamon.

OSMAN, M. A., MITTAL, V. & LUSTI, H. R. 2004. The aspect ratio and gas permeation in polymer-layered silicate nanocomposites. *Macromolecular Rapid Communications,* 25**,** 1145-1149.

PAVLIDOU, S. & PAPASPYRIDES, C. 2008. A review on polymer–layered silicate nanocomposites. *Progress in polymer science,* 33**,** 1119-1198.

POWELL, C. E. & BEALL, G. W. 2006. Physical properties of polymer/clay nanocomposites. *Current Opinion in Solid State and Materials Science,* 10**,** 73-80.

QIAN, D., DICKEY, E. C., ANDREWS, R. & RANTELL, T. 2000. Load transfer and deformation mechanisms in carbon nanotube-polystyrene composites. *Applied Physics Letters,* 76**,** 2868-2870.

QIU, Y.-R. & MATSUYAMA, H. 2010. Preparation and characterization of poly(vinyl butyral) hollow fiber membrane via thermally induced phase separation with diluent polyethylene glycol 200. *Desalination,* 257**,** 117-123.

RAY, S. S., OKAMOTO, K. & OKAMOTO, M. 2003. Structure-property relationship in biodegradable poly(butylene succinate)/layered silicate nanocomposites. *Macromolecules,* 36**,** 2355-2367.

REICHLE, W. T. 1986. Synthesis of anionic clay minerals (mixed metal hydroxides, hydrotalcite). *Solid State Ionics,* 22**,** 135-141.

ROLL BACK MALARIA, W. 2000. Introduction to the strategic plan for capacity development for RBM.

RUBINSTEIN, M. & COLBY, R. H. 2003. Polymer Physics. Oxford University Press.

SHI, Y., KASHIWAGI, T., WALTERS, R. N., GILMAN, J. W., LYON, R. E. & SOGAH, D. Y. 2009. Ethylene vinyl acetate/layered silicate nanocomposites prepared by a surfactant-free method: Enhanced flame retardant and mechanical properties. *Polymer,* 50**,** 3478-3487.

SINHA RAY, S. & OKAMOTO, M. 2003. Polymer/layered silicate nanocomposites: a review from preparation to processing. *Progress in Polymer Science,* 28**,** 1539-1641.

SMITH, J. A. & GALAN, A. 1995. Sorption of nonionic organic contaminants to single and dual organic cation bentonites from water. *Environmental Science and Technology,* 29**,** 685-692.

SONG, S. W. & TORKELSON, J. M. 1995. Coarsening effects on the formation of microporous membranes produced via thermally induced phase separation of polystyrene-cyclohexanol solutions. *Journal of Membrane Science,* 98**,** 209-222.

SORRENTINO, A., GORRASI, G., TORTORA, M. & VITTORIA, V. 2006. Barrier properties of polymer/clay nanocomposites. *Polymer Nanocomposites.*

SPERLING, L. H. 2005. *Introduction to physical polymer science*, John Wiley & Sons.

SRIDHAR, R., NARASIMHA MURTHY, H. N., PATTAR, N., VISHNU MAHESH, K. R. & KRISHNA, M. 2012. Parametric study of twin screw extrusion for dispersing MMT in vinylester using orthogonal array technique and grey relational analysis. *Composites Part B: Engineering,* 43**,** 599-608.

STOCKMEYER, M. R. 1991. Adsorption of organic compounds on organophilic bentonites. *Applied Clay Science,* 6**,** 39-57.

STRAWHECKER, K. E. & MANIAS, E. 2000. Structure and properties of poly(vinyl alcohol)/Na+ montmorillonite nanocomposites. *Chemistry of Materials,* 12**,** 2943-2949.

THENG, B. K. G., CHURCHMAN, G. J., GATES, W. P. & YUAN, G. 2008. Organically modified clays for pollutant uptake and environmental protection. *Soil Mineral Microbe-Organic Interactions: Theories and Applications.*

TJONG, S. C. & MAI, Y. W. 12 Modelling permeability behaviour of polymer nanocomposites. *Physical Properties and Applications of Polymer Nanocomposites.* Woodhead Publishing.

TRAPE, J.-F., TALL, A., DIAGNE, N., NDIATH, O., LY, A. B., FAYE, J., DIEYE-BA, F., ROUCHER, C., BOUGANALI, C., BADIANE, A., SARR, F. D., MAZENOT, C., TOURÉ-BALDÉ, A., RAOULT, D., DRUILHE, P., MERCEREAU-PUIJALON, O., ROGIER, C. & SOKHNA, C. 2011. Malaria morbidity and pyrethroid resistance after the introduction of insecticide-treated bednets and artemisinin-based combination therapies: a longitudinal study. *The Lancet Infectious Diseases,* 11**,** 925-932.

TSAI, F.-J. & TORKELSON, J. M. 1990. Microporous poly(methyl methacrylate) membranes. Effect of a low-viscosity solvent on the formation mechanism. *Macromolecules,* 23**,** 4983-4989.

ULBRICHT, M. 2006. Advanced functional polymer membranes. *Polymer,* 47**,** 2217-2262.

UTRACKI, L. A. 2004. *Clay containing polymeric nanocomposites -Part 2*, Shrewsbury : Rapra Technology Ltd.

VACCARI, A. 1998. Preparation and catalytic properties of cationic and anionic clays. *Catalysis Today,* 41**,** 53-71.

VAN DE WITTE, P., DIJKSTRA, P. J., VAN DEN BERG, J. W. A. & FEIJEN, J. 1996. Phase separation processes in polymer solutions in relation to membrane formation. *Journal of Membrane Science,* 117**,** 1-31.

VANDEWEERDT, P., BERGHMANS, H. & TERVOORT, Y. 1991. Temperature-concentration behavior of solutions of polydisperse, atactic poly(methyl methacrylate) and its influence on the formation of amorphous, microporous membranes. *Macromolecules,* 24**,** 3547-3552.

VANEGAS, M. E., QUIJADA, R. & SERAFINI, D. 2009. Microporous membranes prepared via thermally induced phase separation from metallocenic syndiotactic polypropylenes. *Polymer,* 50**,** 2081-2086.

WAGENER, R. & REISINGER, T. J. 2003a. A rheological method to compare the degree of exfoliation of nanocomposites. *Polymer,* 44**,** 7513-7518.

WAGENER, R. & REISINGER, T. J. G. 2003b. A rheological method to compare the degree of exfoliation of nanocomposites. *Polymer,* 44**,** 7513-7518.

WANG, C. C., JUANG, L. C., LEE, C. K., HSU, T. C., LEE, J. F. & CHAO, H. P. 2004. Effects of exchanged surfactant cations on the pore structure and adsorption characteristics of montmorillonite. *Journal of Colloid and Interface Science,* 280**,** 27-35.

WANG, J., CALHOUN, M. D. & SEVERTSON, S. J. 2008. Dynamic rheological study of paraffin wax and its organoclay nanocomposites. *Journal of Applied Polymer Science,* 108**,** 2564-2570.

WELTY, J. R., WICKS, C.E., WILSON, R.E. 1984. *Fundamentals of momentum, heat and mass transfer*, New York : John Wiley & Sons.

WILLIAMS, J. M. & MOORE, J. E. 1987. Microcellular foams: phase behaviour of poly(4-methyl-1-pentene) in diisopropylbenzene. *Polymer,* 28**,** 1950-1958.

XI, Y., MARTENS, W., HE, H. & FROST, R. L. 2005. Thermogravimetric analysis of organoclays intercalated with the surfactant octadecyltrimethylammonium bromide. *Journal of Thermal Analysis and Calorimetry,* 81**,** 91-97.

XU, B., ZHENG, Q., SONG, Y. & SHANGGUAN, Y. 2006. Calculating barrier properties of polymer/clay nanocomposites: Effects of clay layers. *Polymer,* 47**,** 2904-2910.

XU, R., MANIAS, E., SNYDER, A. J. & RUNT, J. 2001. New biomédical poly(urethane urea)-layered silicate nanocomposites. *Macromolecules,* 34**,** 337-339.

YANO, K., USUKI, A. & OKADA, A. 1997. Synthesis and properties of polyimide-clay hybrid films. *Journal of Polymer Science, Part A: Polymer Chemistry,* 35**,** 2289-2294.

YAVE, W., QUIJADA, R., ULBRICHT, M. & BENAVENTE, R. 2005. Syndiotactic polypropylene as potential material for the preparation of porous membranes via thermally induced phase separation (TIPS) process. *Polymer,* 46**,** 11582-11590.

YÍLMAZ, N. & YAPAR, S. 2004. Adsorption properties of tetradecyl- and hexadecyl trimethylammonium bentonites. *Applied Clay Science,* 27**,** 223-228.

ZANETTI, M., LOMAKIN, S. & CAMINO, G. 2000. Polymer layered silicate nanocomposites. *Macromolecular Materials and Engineering,* 279**,** 1-9.

ZENG, Q. H., YU, A. B., LU, G. Q. & PAUL, D. R. 2005. Clay-based polymer nanocomposites: Research and commercial development. *Journal of Nanoscience and Nanotechnology,* 5**,** 1574-1592.

ZHANG, W. A., CHEN, D., ZHAO, Q. & FANG, Y. E. 2003. Effects of different kinds of clay and different vinyl acetate content on the morphology and properties of EVA/clay nanocomposites. *Polymer,* 44**,** 7953-7961.

ZHU, L., REN, X. & YU, S. 1998. Use of cetyltrimethylammonium bromide-bentonite to remove organic contaminants of varying polar character from water. *Environmental Science and Technology,* 32**,** 3374-3378.

ZHU, L., ZHU, R., XU, L. & RUAN, X. 2007. Influence of clay charge densities and surfactant loading amount on the microstructure of CTMA-montmorillonite hybrids. *Colloids and Surfaces A: Physicochemical and Engineering Aspects,* 304**,** 41-48.

ZIDELKHEIR, B. & ABDELGOAD, M. 2008. Effect of surfactant agent upon the structure of montmorillonite: X-ray diffraction and thermal analysis. *Journal of Thermal Analysis and Calorimetry,* 94**,** 181-187.

ВАЛАC, C. M. 1985. *Phase equilibria in chemical engineering*, Butterworth.

APPENDIX 1: Derivation of equation (13)

We assume that the size of each segment in lattice model is equal to the volume of a solvent molecule V_0 and x is the number of volume segments in a polymer molecular chain.

Therefore, $V_1 = N_1 V_0$ and $V_2 = x N_2 V_0$

Therefore, $\dfrac{V_1}{V_2} = \dfrac{N_1}{x \, N_2}$

Also, $n_1 = \dfrac{N_1}{N_A}$ and $n_2 = \dfrac{N_2}{N_A}$

Since, $V_1 = \dfrac{V_2 N_1}{x \, N_2}$

Adding V_2 on both sides, $V_1 + V_2 = \left(\dfrac{N_1}{x \, N_2} + 1 \right) V_2$

But $\dfrac{V_2}{V_1 + V_2} = \dfrac{1}{\left(\dfrac{N_1}{x \, N_2} + 1 \right)} = \phi_2$

Therefore, $\phi_2 = \dfrac{x \, N_2}{N_1 + x \, N_2}$

In terms of number of moles, the above equation can be written as,

$$\phi_2 = \frac{x \, n_2}{n_1 + x \, n_2}$$

Similarly, $\phi_1 = 1 - \phi_2$

Therefore, $\phi_1 = 1 - \dfrac{x \, n_2}{n_1 + x \, n_2} = \dfrac{n_1}{n_1 + x \, n_2}$ or $\phi_1 = \dfrac{N_1}{N_1 + x \, N_2}$

We know from Equation 13 (F-H equation)

$$\Delta G_{mix} = RT [n_1 \ln \phi_1 + n_2 \ln \phi_2 + n_1 \phi_2 \chi]$$

Therefore,

$$\Delta G_{mix} = RT[\phi_1(n_1 + x\,n_2)ln\phi_1 + \frac{\phi_2}{x}(n_1 + x\,n_2)\ln\phi_2 + \phi_1(n_1 + x\,n_2)\phi_2\chi]$$

If we assume that the entire lattice is equals to one mole, then the above equation becomes

$$\Delta G_{mix} = RT[\phi_1 ln\phi_1 + \frac{\phi_2}{x}\ln\phi_2 + \phi_1\phi_2\chi]$$

or

$$\Delta G_{mix} = RT\left[(1 - \phi_2)\ln(1 - \phi_2) + \frac{\phi_2}{x}\ln\phi_2 + (1 - \phi_2)\phi_2\chi\right]$$

Convert the value of heat of fusion or heat of crystallization to Joules per mole

Since we know that,

$$x = \frac{M_{n.2}/\rho_2}{M_1/\rho_1}$$

where M_n is the number average molecular mass of the polymer.

Therefore,

$$\Delta H_u = \frac{M_{w.2}}{x}$$

or

$$\Delta H_u = \frac{M_{w.2}M_1\rho_2}{M_{n.2}\rho_1} = D_{M.2}\frac{M_1\rho_2}{\rho_1}$$

where $M_{w.2}$ is the weight average molecular mass of the polymer and $D_{M.2}$ is the Molar mass dispersity or degree of polymerization of the polymer.